Journal of Umm Al-Qura University for Engineering and Architecture (2025) 16:1806–1838
https://doi.org/10.1007/s43995-025-00211-3

ORIGINAL ARTICLE

Comparative analysis of machine learning models and standard codes for predicting compressive strength in hollow block masonry

Navaratnarajah Sathiparan[1] · Pratheeba Jeyananthan[2]

Received: 6 April 2025 / Accepted: 23 August 2025 / Published online: 23 September 2025

Abstract

This study employs machine learning models to predict the compressive strength of hollow block masonry and examines the key factors that influence this strength. Accurate prediction of its compressive strength is crucial for ensuring the safety of structures. The study expands the dataset to include all relevant factors affecting (compressive strength of masonry units and mortar, mortar thickness, prism height-to-thickness ratio, length-to-thickness ratio, net-to-gross area ratio of hollow blocks, and bedding type). It compares the prediction accuracy of existing standard code equations and published empirical expressions with machine learning models. The findings demonstrate that machine learning models, particularly XGBoost (XGB), outperform standard code equations and other models in predicting compressive strength. The XGB model achieves high accuracy (R^2 >0.92) and low error (RMSE < 2.14 MPa) for both training and validation datasets. Feature importance analysis reveals that the strength of the masonry units is the most dominant factor affecting compressive strength, followed by mortar strength and the prism's height-to-thickness ratio. Mortar thickness, length-to-thickness ratio, net-to-gross area ratio, and bedding type have a lesser influence on the overall strength. This study highlights the potential of XGB for accurately and efficiently predicting the compressive strength of hollow block masonry. Engineers can optimize the material selection, wall thickness, and design for improved structural performance by focusing on the most critical factors identified through feature importance analysis.

Keywords Hollow block masonry · Machine learning · Prediction model · SHAP analysis · Feature importance

Abbreviations

f_b	Compressive strength of the masonry unit
f_m	Compressive strength of the mortar
f_{mp}	Compressive strength of the hollow block masonry prisms
t_m	Thickness of the mortar
H/t	Height-to-width ratio of the prisms
L/t	Length-to-width ratio of the prisms
α	Net-to-gross area ratio of the masonry unit
R^2	Coefficient of determination
RMSE	Root Mean Squared Error
MAE	Mean Absolute Error
SI	Scatter Index
ANN	Artificial neural networks
BT	Boosted tree regression
KNN	K-nearest neighbors
RF	Random Forest regression
XGB	Extreme Gradient Boosting
SVR	Support vector regression
SHAP	SHapley Additive exPlanations

1 Introduction

Masonry structures are known for their exceptional longevity, withstanding harsh weather conditions and resisting fire for extended periods. It often utilizes locally sourced materials, reducing transportation costs and environmental impact. The thermal mass properties can also contribute to energy efficiency [1, 2]. Hollow block masonry, a specific type of masonry construction that utilizes hollow concrete blocks, offers additional benefits, including cost-effectiveness,

✉ Navaratnarajah Sathiparan
sakthi@eng.jfn.ac.lk

[1] Department of Civil Engineering, Faculty of Engineering, University of Jaffna, Jaffna, Sri Lanka

[2] Department of Computer Engineering, Faculty of Engineering, University of Jaffna, Jaffna, Sri Lanka

lightweight construction, and improved insulation. Conversely, some limitations exist, including lower tensile strength, increased moisture susceptibility, and reduced fire resistance [3]. Therefore, carefully considering its limitations and employing appropriate design strategies is crucial for the successful implementation of this approach [4].

Accurate prediction of the compressive strength of hollow block masonry is crucial to ensure that the masonry structure can safely bear the intended loads. This prevents potential failures and safeguards building occupants. Predicting strength allows engineers to optimize material selection and wall thickness [5]. Beyond ensuring structural safety and optimizing material use, accurately assessing compressive strength is vital for the development and implementation of new engineering practices. For example, recent studies have explored methods to enhance the compressive properties of masonry, such as the use of confining techniques. Nasrollahzadeh and Zare [6] investigated the use of polymeric straps to confine axially loaded adobe masonry columns, demonstrating a practical approach to improving their strength for real-world applications. Such research underscores the importance of understanding and predicting compressive strength to enhance the application of masonry in diverse structural contexts. Using the right amount of material for the required strength reduces construction costs and unnecessary weight on the foundation. Strength prediction methods can be utilized during construction to evaluate the quality of the masonry work and identify potential issues early on. Destructive testing of masonry prisms provides the most accurate strength data. However, this method is time-consuming, expensive, and limits the number of samples that can be tested [7].

Standard codes are beneficial for predicting the compressive strength of hollow block masonry. Codes do not directly indicate the masonry strength. Instead, they provide reduction factors based on factors such as masonry unit strength, mortar type (strength and joint thickness), and the dimensions of the prism or wallet [8]. Conversely, empirical equations rely on historical data and established relationships between block strength, mortar strength, and geometrical properties. Although several empirical equations are proposed for solid block masonry [7, 9–16] and grouted masonry [17–22], few equations are proposed to predict the compressive strength of hollow block masonry. While empirical equations offer a simple approach, they are often based on averaged data and may not capture the complex interactions between all influencing factors. Additionally, these equations may not account for influential factors such as the net-to-gross area ratio of the hollow block and the aspect ratio (length-to-thickness ratio) of the prisms. This can lead to inaccurate predictions for specific cases [23].

While various machine learning models have been successfully applied to predict material properties, other methods are also essential candidates for structural engineering research [24, 25]. For instance, fuzzy logic has emerged as a valuable tool for complex analyses, such as assessing seismic fragility and managing construction quality. Kiani and Nasrollahzadeh [26] demonstrated the application of a fuzzy logic approach for seismic fragility analysis of RC frames, showcasing its utility in addressing uncertainty and making informed decisions in earthquake-induced damage assessment. This exemplifies how different ML methods can be leveraged to address a diverse range of challenges in structural engineering. This approach utilizes algorithms that learn from large datasets to identify patterns and relationships between input variables (e.g., component strengths, geometry) and the target output (compressive strength). Machine learning models can offer high accuracy and consider a broader range of factors compared to traditional methods [27].

Recent studies have demonstrated the effectiveness of various ML models in predicting the compressive strength of masonry units and assemblies. For instance, Artificial Neural Networks (ANNs) and Random Forests have been successfully employed to predict the compressive strength of masonry units made from alternative materials such as geopolymer bricks utilizing rice husk ash and eggshell ash. These models achieved high prediction accuracy, with an R^2 value of 0.95 [5, 28]. Similarly, ANN models have outperformed traditional empirical methods in predicting the compressive strength of masonry prisms, providing significant predictive accuracy [5, 29]. In the case of Compressed Earth Blocks (CEBs), Genetic Programming and Fuzzy Logic have been integrated into soft computing models to enhance the prediction of compressive strength, addressing the variability in material composition and manufacturing conditions [30, 31]. Furthermore, SHapley Additive Explanations (SHAP) have been utilized to interpret the ML models by revealing which factors—such as material properties, dimensions, and compaction pressure—most significantly affect the predicted compressive strength of masonry materials [32]. This added interpretability enables researchers to understand better the impact of individual parameters on the performance of masonry units, aiding in the optimization of material selection and design [33]. The potential for sustainability in masonry is further supported by ML's application to eco-friendly alternatives, such as alkali-activated masonry blocks. Studies show that these blocks, made from waste products such as quarry waste, rice husk ash, and eggshell ash, offer reduced carbon emissions and promote resource efficiency while maintaining or even improving their mechanical properties [28]. Machine learning has also been applied to grouted masonry systems, where ANN models effectively predict compressive strength by accounting for factors such as the compressive strength of the grout, mortar, and the geometry of the blocks [34]. Additionally, studies on unreinforced masonry walls highlight the use of ML algorithms like Gradient Boosting Machines (GBM) and Extreme Gradient Boosting (XGBoost) to predict shear strength, revealing the potential of these models for assessing structural integrity in masonry buildings [31]. In comparison, traditional methods often rely on empirical equations, which have limitations in accuracy. Machine learning models offer an alternative that can account for a broader range of variables and achieve superior prediction performance [31]. Despite the successes of these models, challenges remain in standardizing ML approaches for masonry applications, especially given the variability in material properties and the complexity of masonry structures.

Several studies focus on predicting compressive strength using machine learning models [35–37]. These studies have identified two fundamental limitations in this area: limited data availability and the exclusion of potentially influential factors. Biased or unreliable predictions can arise from inaccurate or incomplete training data, as the quality and quantity of the data significantly influence the model's accuracy. Models that utilize large datasets encompassing all relevant factors (component strengths, geometry, etc.) can provide more accurate and reliable predictions. Considering the research gap mentioned above, the present study expanded the dataset further. It included all the influencing factors (strength of masonry unit, strength of mortar, thickness of mortar, height-to-thickness ratio of the prism, length-to-thickness ratio of the prism, net-to-gross area ratio of the hollow block, and bedding type) used to predict the compressive strength of hollow block masonry. The prediction accuracy of the equation provided by standard code, the empirical expression proposed by published literature, and machine models is compared. Based on performance indicators, the best model was selected, and the study was further extended to conduct a sensitivity analysis and assess the importance of these parameters on the compressive strength of hollow block masonry.

2 Methodology

Figure 1 presents the systematic workflow followed in this study for predicting the compressive strength of hollow block masonry using machine learning techniques. The figure outlines the six main steps of the process, each contributing to the development and validation of the prediction model.

- Step 1: The first step involves collecting a comprehensive dataset from various published studies and databases, such as Web of Science, Scopus, and Google Scholar. This dataset contains relevant variables.
- Step 2: Statistical analysis is performed to calculate various measures, including the mean, standard deviation, skewness, and kurtosis, for each variable. This helps in understanding the distribution and characteristics of the dataset. Correlation analysis is also conducted to examine the relationships between the independent variables and the compressive strength of the masonry.
- Step 3: Before training machine learning models, the compressive strength of the hollow block masonry is predicted using traditional methods provided by existing codes (Eurocode 6 and AS 3700). These predictions are based on standard formulas that incorporate parameters such as masonry unit strength, mortar type, and prism geometry. The purpose of this step is to establish a baseline prediction. By comparing machine learning models to traditional code predictions, we can assess whether machine learning methods provide improvements over standard code-based estimations. This step serves as a reference for the performance of more advanced techniques and justifies the choice of machine learning models for this study.
- Step 4: Machine learning models are developed and trained. Six different algorithms are used: Artificial Neural Networks (ANN), K-Nearest Neighbors (KNN), Random Forest Regression (RF), Boosted Tree Regression (BT), Extreme Gradient Boosting (XGB), and Support Vector Regression (SVR). The models are trained using the dataset, with hyperparameters optimized to achieve the best predictive performance.
- Step 5: To validate the performance of the machine learning models, a ten-fold cross-validation technique is employed. This ensures that the models' generalizability is assessed and minimizes the risk of overfitting. Performance metrics such as R^2, RMSE, MAE, and Scatter Index (SI) are used to compare the accuracy of each model. These metrics assess the models' ability to predict the compressive strength of hollow block masonry and the degree to which the predicted values align with the actual data.
- Step 6: Sensitivity analysis is conducted using SHAP (SHapley Additive exPlanations) values. This step helps identify which input variables have the most significant influence on the predicted compressive strength. The analysis provides insights into the relationship between material properties, geometric factors, and compressive strength, guiding future decisions in masonry design and material selection.

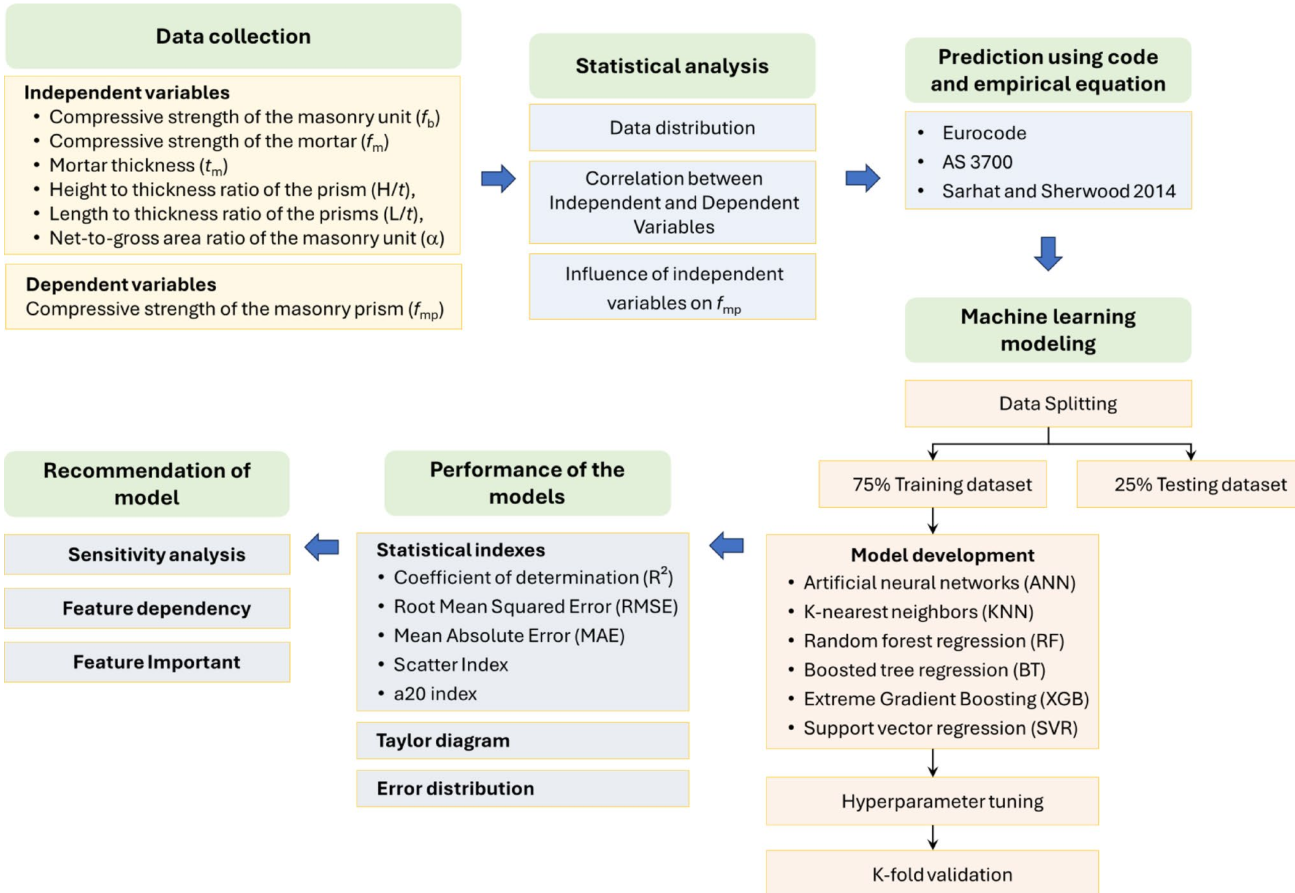

Fig. 1 Flow chart for the prediction of compressive strength of hollow block masonry using machine learning models

2.1 Data collection

The dataset was compiled through a comprehensive literature review using established databases, including Web of Science, Scopus, and Google Scholar. Their search focused on identifying research related to the compressive strength of hollow block masonry. They specifically targeted studies that included these terms in the title, abstract, or keywords. Following the initial search, a meticulous screening process was conducted to eliminate duplicates, ensuring the collection of unique and original data for further analysis. Details relevant to building machine learning models were then extracted and compiled in Table 1. Key factors identified for model development included: compressive strength of masonry unit (f_b), compressive strength of mortar (f_m), thickness of the bed mortar (t_m), height-to-thickness of the prism (H/t), length-to-thickness of the prism (L/t), net-to-gross area ratio of hollow block (α), bedding type, and compressive strength of hollow block masonry (f_{mp}). With a robust dataset of 511 data points, the study established a solid foundation for subsequent analysis. The assembled database covers masonry prisms and wallets with a solid area ranging from 35 to 90% of the gross area. Eurocode 6 classifies masonry units into distinct "Groups" based on material used and void content, which are essential for determining the structural performance of masonry. These groups are crucial as they guide the selection of appropriate design parameters and influence the calculation of compressive strength for masonry structures. In the dataset used for this study, the hollow block masonry units were categorized into three groups based on Eurocode 6 guidelines. Specifically, Group 1: corresponds to masonry units with a void percentage less than 25%, Group 2: represents masonry units with moderate void percentage (25–55%), and Group 3: includes high void percentage (55–70%). There are 11.3% blocks categorized as "Group 1", 87.9% as "Group 2", and 0.8% as "Group 3", as per Eurocode 6 [38]. Most of the prims used 10 mm thick mortar for the bed joint (55.0%), and 37.4% of prisms used less than 10 mm mortar for the bed joint. The percentages of full bedding and face shell bedding are 74.2% and 25.8%, respectively.

Although bedding type is a categorical variable, it was included as an input parameter in the machine learning models through the use of one-hot encoding. This technique transforms categorical variables into binary (0 or 1) variables, with each category of bedding type (e.g., complete

Table 1 Summary of the dataset for independent and dependent variables collected from published literature

Reference	f_b (MPa)	f_m (MPa)	t_m (mm)	H/t	L/t	α	Bedding	f_{mp} (MPa)	Data
Casali et al. [39]	20.9–22.2	6.9–15.4	10	4.21	2.79	0.56–0.66	FB	8.5–15.9	8
Sathiparan et al. [40]	1.8–4.5	5.1	10	3.17	1.96	0.56–0.84	FB	1.2–1.9	4
Al-Amoudi and Alwathaf [41]	18.1	17.6	10	6.30–6.34	4.00	0.74	FS	14.1–15.4	6
Sarhat and Sherwood [8]	9.0–45.8	2.9–26.6	5–18	1.63–6.26	0.81–4.32	0.51–0.74	FSB, FB	6.7–31.0	243
Zhou et al. [42]	23.2–36.8	5.6–13.7	10	3.11–5.21	2.05	0.54	FB	10.2–27.0	12
Valdameri et al. [43]	7.2–8.4	2.6–6.4	10	6.30–6.33	4.00	0.35–0.39	FB	3.7–4.8	4
Zavalis et al. [44]	17.0–22.9	6.6–33.0	5–15	5.37–8.31	1.39–2.08	0.80–0.81	FB	11.6–16.6	15
Fonseca et al. [45]	40.7–74.9	14.0–32.0	10	2.79	2.79	0.46	FB	19.6–44	48
Liu et al. [46]	5.3–10.5	3.1–14.8	10	2.46	1.63	0.66	FB	2.7–8.6	9
Caldeira et al. [47]	16.3–45.6	5.6–18.3	5–20	2.74–2.89	2.81–2.85	0.56–0.59	FB	5.6–22.5	24
Abdel Rahman and Gala [48]	37.4–39.0	21.4	5–10	2.05–2.06	2.05–2.06	0.56–0.57	FB	24.1–26.6	6
Li et al. [49]	10.2	8.5–15.8	8	6.32	4.00	0.58	FB	5.4–9.1	10
Zahra et al. [50]	11.3–15.6	2.5–17.1	10	4.16–6.56	2.05–4.33	0.56–0.74	FSB, FB	5.8–9.3	7
Syiemionga and Marthong [51]	2.5–3.2	7.3–27.0	10	6.16–7.55	3.63–3.85	0.84–0.90	FB	1.7–2.8	41
Chávez-Gómez et al. [52]	11.3	17.1	0	2.05–4.16	2.05	0.56	FSB, FB	6.2–13.4	59
Elmeligy et al. [53]	39.5	37.3–40.7	5	3.11	2.06	0.64	FB	23.0–38.1	15
Overall	1.8–74.9	2.5–40.7	5–20	1.63–8.31	0.81–4.33	0.35–0.9	FSB, FB	1.2–44	511

FSB: face shell bedding, FB: Full bedding

bedding and face-shell bedding) represented as a separate binary feature. This encoding ensures that the models can adequately capture the influence of bedding type on the compressive strength of hollow block masonry while maintaining its categorical nature. In these studies, the compressive strength of hollow block masonry (f_{mp}) refers to the maximum load-bearing capacity of a masonry prism, typically determined under axial compressive loading. The load is applied vertically along the height of the masonry prism, which is a direction perpendicular to the bed joints. This testing orientation is critical because it reflects the actual load distribution within a masonry wall, where the weight of the structure is transmitted vertically through the masonry units and mortar joints.

Figure 2 visually illustrates the distribution of key parameters within the dataset. Various statistical measures were calculated for each variable to gain a deeper understanding of the data's characteristics. These measures include mean, minimum and maximum values, standard deviation, skewness, and kurtosis. The analysis of skewness and kurtosis provides valuable insights into the shape of the data distribution of the parameters. A positive skewness was observed for all parameters except the mortar thickness. This suggests a tendency for the data to have a longer tail towards higher values for these properties. The mortar thickness data has a skewness close to zero, suggesting a more symmetrical distribution around the average value. Kurtosis describes the "peakedness" of the data distribution. The mortar thickness data has a higher kurtosis value, indicating a sharper peak with fatter tails. This means there might be a concentration of data points around the average mortar thickness, with a few instances of very thin or very thick mortar layers used in the studies.

2.1.1 Correlation analysis

Statistical analysis was performed to investigate the relationships between chosen parameters and the compressive strength of hollow block masonry (f_{mp}). As shown in Fig. 3, the results indicate no strong correlations between independent variables. However, a clear positive correlation emerged between the f_b and f_{mp}. The correlation coefficient (R) of 0.89 suggests a substantial increase in f_{mp} with higher f_b values. Similarly, a positive correlation, although weaker ($R=0.47$), was observed between the f_m and f_{mp}. Interestingly, tm, H/t, L/t, and α parameters exhibited negative correlations ($R = -0.18, -0.46, -0.34$, and -0.56, respectively) with f_{mp}. This suggests that increasing these parameters tends to decrease the compressive strength of the masonry.

Figure 4 depicts the influence of various factors on the compressive strength of hollow masonry. The contours shown in Fig. 5 are generated using a method based on clustering and interpolation techniques. Specifically, the contours represent regions of constant compressive strength, derived from a combination of multiple input parameters. The contours are constructed by first grouping the data into clusters based on similarities in these parameters using a clustering algorithm. Following clustering, interpolation techniques are applied to the clustered data points to estimate continuous values across the entire dataset. These interpolated values are then plotted as contours, highlighting areas where compressive strength is constant. This approach allows us to visually assess the impact of multiple factors on

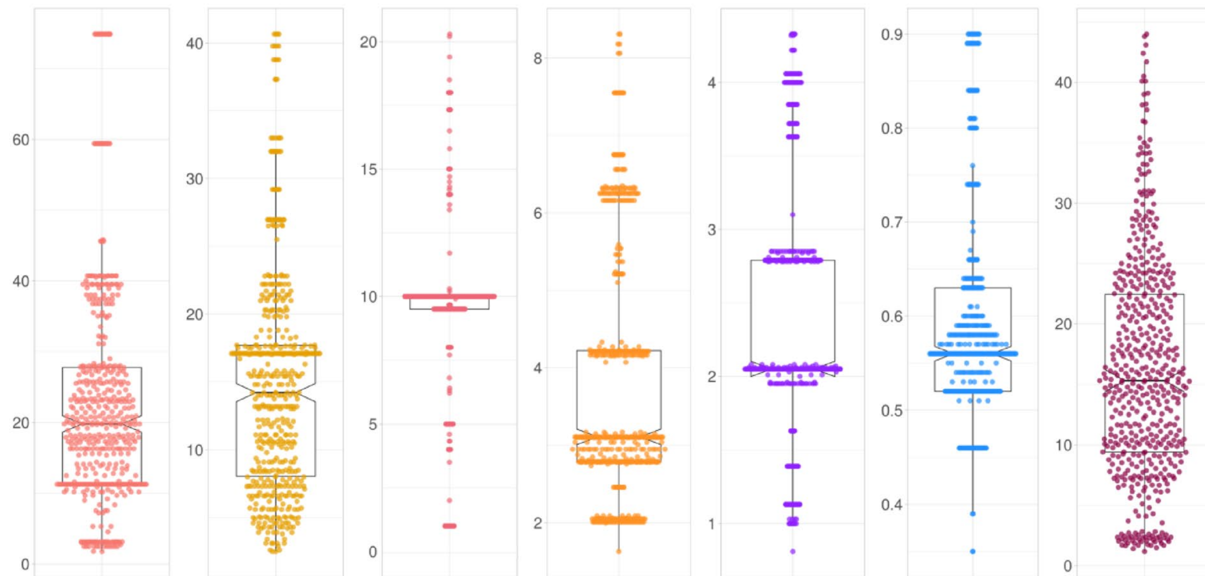

	f_b (MPa)	f_m (MPa)	t_m (mm)	H/t	L/t	α	f_{mp} (MPa)
Minimum	1.77	2.50	1.00	1.63	0.81	0.35	1.18
Maximum	74.90	40.67	20.30	8.31	4.33	0.90	44.00
Average	22.91	14.87	9.33	3.81	2.45	0.59	16.22
Std	15.76	8.22	3.17	1.59	0.85	0.11	9.15
Skewness	1.48	0.93	-0.47	0.97	0.53	1.34	0.54
Kurtosis	2.45	0.82	2.99	-0.15	-0.43	1.29	-0.04

Fig. 2 Data distribution and summary of statistical measures

the compressive strength and understand the relationships between them more intuitively. The clustering method used helps identify distinct patterns in the data. At the same time, the interpolation provides a smooth representation of these patterns across the entire parameter space, aiding in a better understanding of how the various factors influence the compressive strength of hollow block masonry.

The strong positive correlation between the compressive strength of the masonry unit (f_b) and the overall compressive strength of the masonry prism (f_{mp}) is consistent with principles of structural mechanics. The compressive strength of the masonry unit governs the load-bearing capacity of the structure, as it is the primary element resisting axial compressive forces [7]. In masonry, the overall strength of the prism is primarily dictated by the strength of the individual units, which are responsible for carrying the majority of the load. The correlation between mortar strength (f_m) and compressive strength (f_{mp}), though positive, is weaker, reflecting the secondary role of mortar in the load-bearing capacity. Mortar serves as a bonding agent between blocks, facilitating load transfer. However, excessive mortar thickness may result in weak points that limit its effectiveness, as thicker mortar layers reduce the direct contact between blocks, affecting the overall strength. These findings are supported by research on the behavior of masonry under compressive loading, where the interfacial bond between mortar and blocks significantly influences the strength of masonry walls. The negative correlations between compressive strength and parameters like mortar thickness (tm), height-to-thickness ratio (H/t), and length-to-thickness ratio (L/t) align with structural considerations. For example, as the H/t ratio increases (indicating slender prisms), the masonry becomes more susceptible to buckling and failure under compression. Similarly, larger mortar thickness can weaken the interlocking of the blocks, leading to reduced strength. The α value represents the proportion of solid material in the block compared to voids. A higher α value (indicating a more solid material) generally leads to a stronger prism.

2.2 Machine learning models

In this study, six machine learning algorithms were employed to predict the compressive strength of hollow block masonry. Each model was selected for its ability to handle complex, nonlinear relationships between the input variables and the target variable, which includes compressive strength, mortar thickness, masonry unit strength, and various geometric parameters. The architecture of each machine learning model is illustrated in Fig. 5. Below is a detailed description of the machine learning models used:

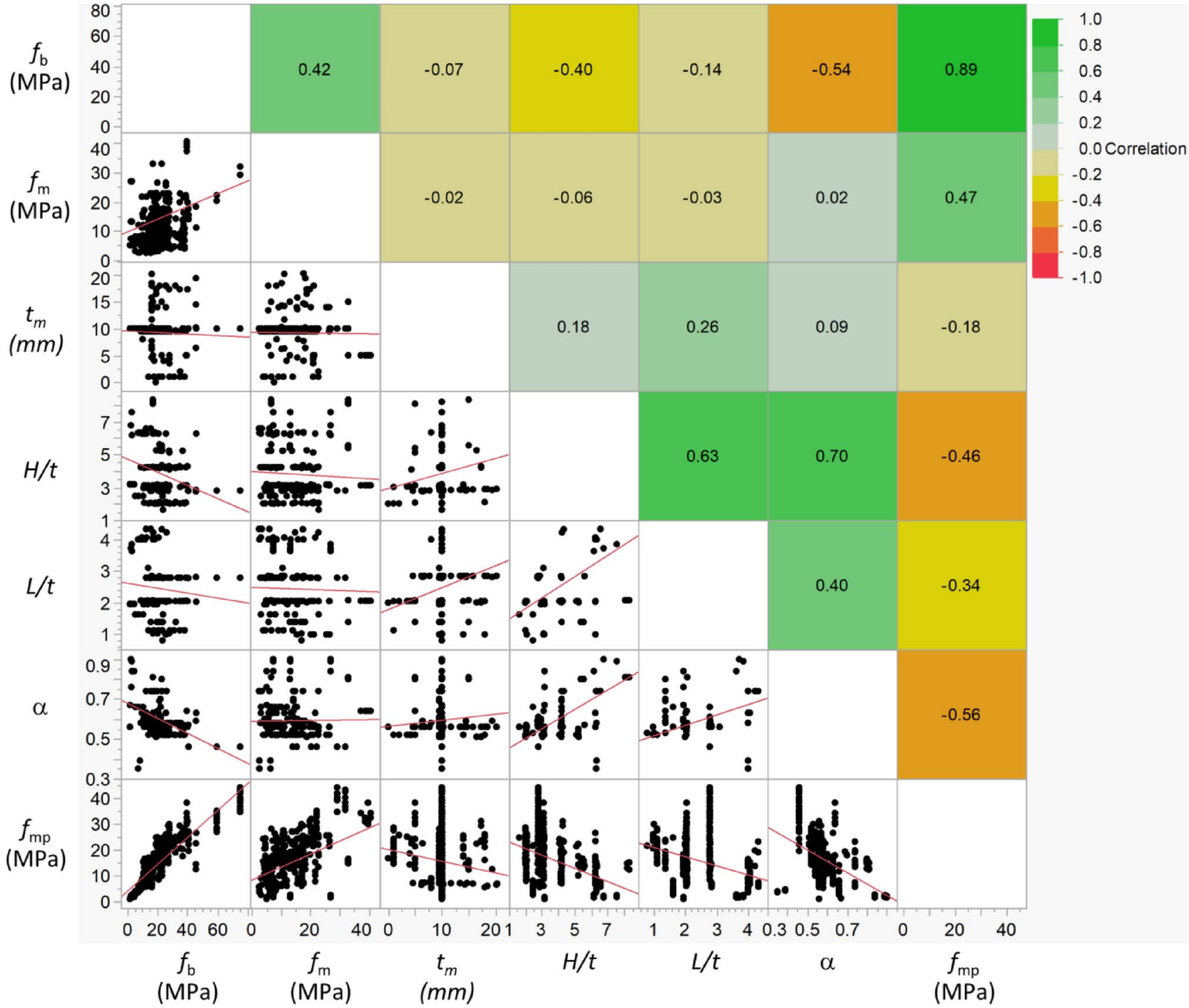

Fig. 3 Correlation analysis between independent and dependent variables

2.2.1 Artificial neural networks (ANN)

Artificial Neural Networks (ANNs) are inspired by the structure of the human brain, with interconnected layers of neurons that process information. In this study, the ANN model used a feedforward architecture with backpropagation for training. The model learns from the data by adjusting the weights of the connections between neurons in a way that minimizes prediction errors. ANNs are capable of capturing complex relationships in data, including nonlinear interactions between the input variables [54]. This makes them particularly effective when the relationships between parameters, such as compressive strength and material properties, are not linear [55]. ANNs require careful tuning of hyperparameters (such as the number of layers and neurons), and they may suffer from overfitting if the training dataset is not sufficiently large or diverse.

2.2.2 K-Nearest neighbors (KNN)

K-Nearest Neighbors (KNN) is a simple, instance-based learning algorithm. It predicts the target variable by finding the k nearest training examples in the feature space and averaging their corresponding output values. The model uses a distance metric (typically Euclidean distance) to measure the proximity between points in the feature space [56]. KNN is easy to implement and interprets well. It performs well when the data has a clear clustering pattern and is non-parametric, meaning it does not make any assumptions about the data distribution. KNN can be computationally expensive for large datasets, as it requires calculating the distance between the query point and all training points. Additionally, its performance can degrade with high-dimensional data due to the curse of dimensionality [57].

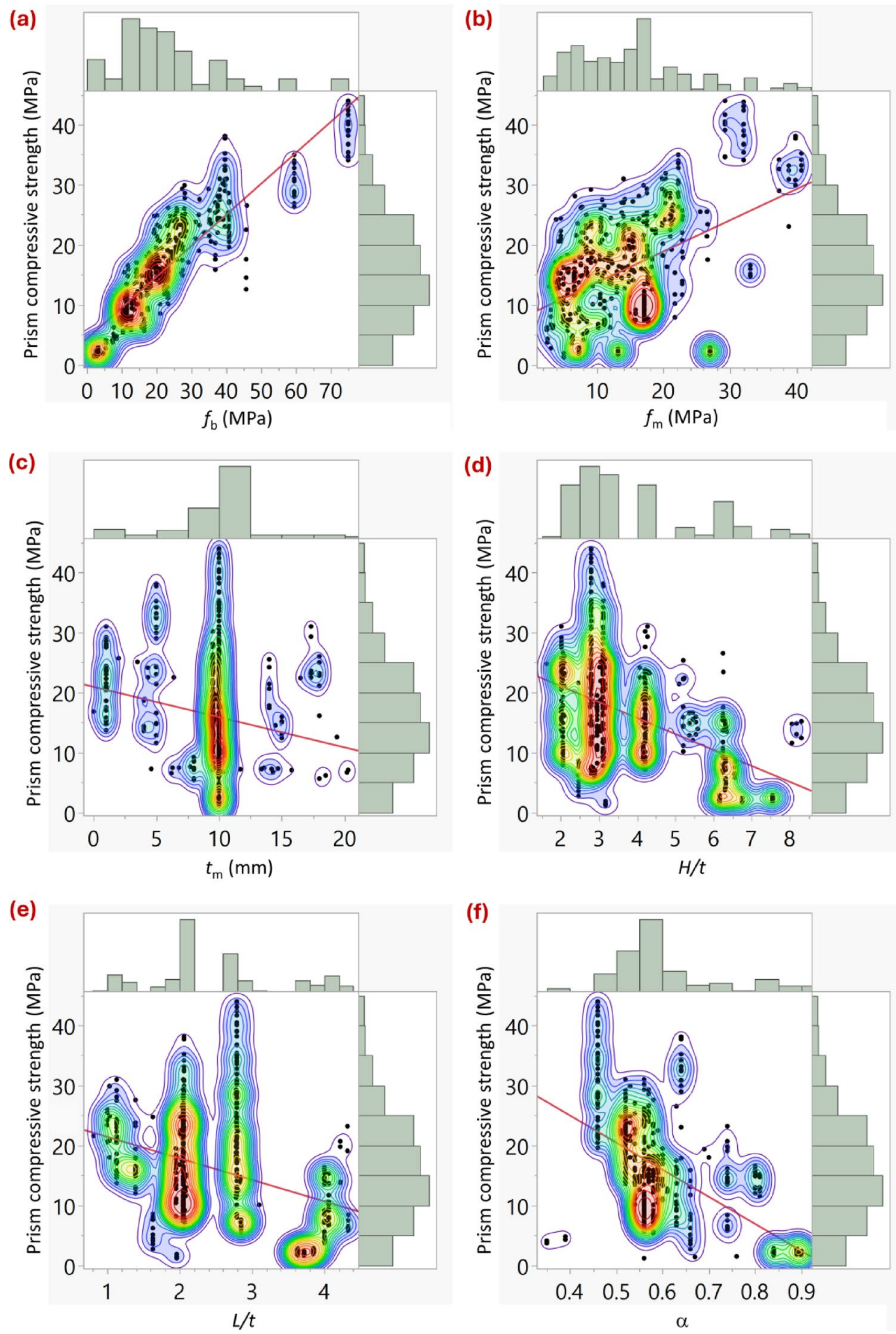

Fig. 4 Effect of materials properties and geometrical properties on compressive strength of hollow block masonry

2.2.3 Random forest (RF)

Random Forest is an ensemble learning method that combines multiple decision trees to improve predictive accuracy. Each tree is trained on a random subset of the data, and the final prediction is made by averaging the predictions from all individual trees. The randomness introduced in the training process helps prevent overfitting. Random Forest handles large datasets and high-dimensional spaces well and is less prone to overfitting than a single decision tree. It can also assess feature importance, making it useful for feature selection and optimization. While Random Forest performs well for many types of data, it can be less interpretable than simpler models, such as decision trees. It also requires tuning of the number of trees and other parameters to achieve optimal performance [58].

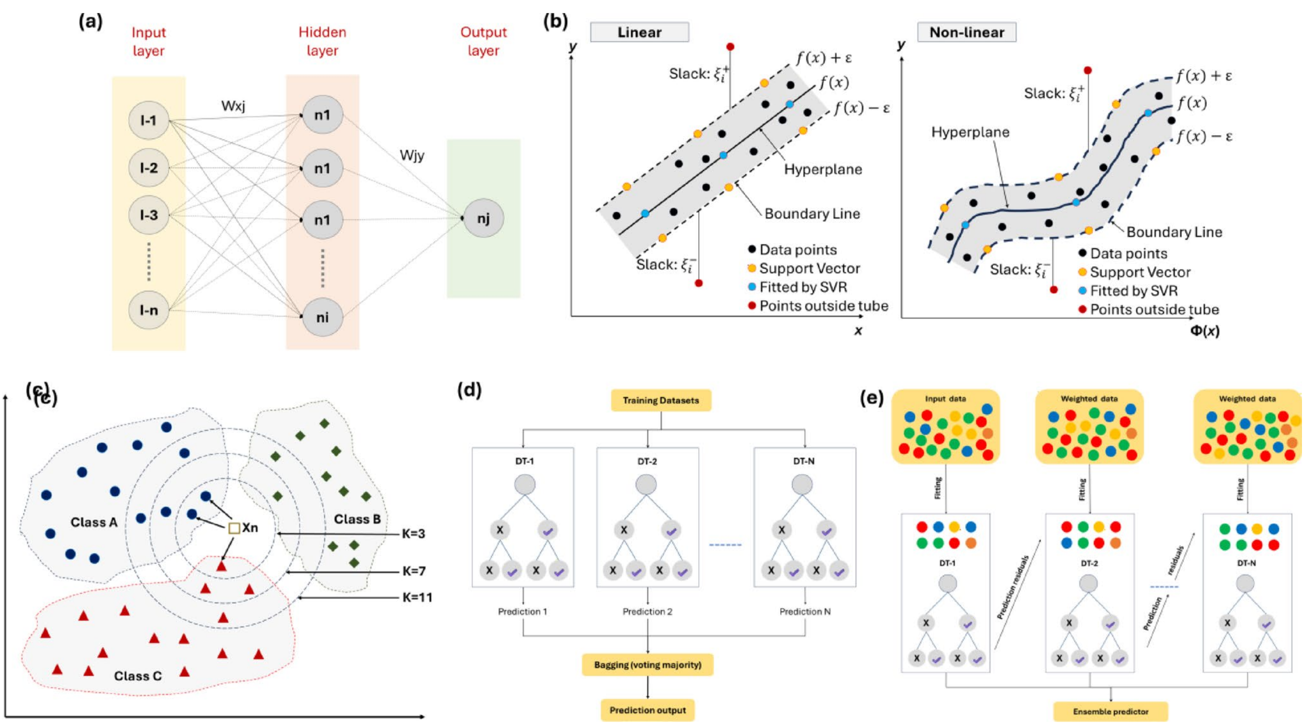

Fig. 5 Concept of machine learning models (**a**) ANN, (b) SVR, (**c**) KNN, (**d**) Random Forest, and (**e**) Boosting decision tree ensemble

2.2.4 Boosted trees (BT)

Boosted Trees combine the predictions of several weak learners (typically shallow decision trees) to create a strong learner. Each tree in the sequence is trained to correct the errors made by the previous tree. The most popular boosting algorithm, Gradient Boosting, is used in this study. Boosted Trees are highly effective for a variety of regression tasks, as they iteratively improve prediction accuracy. They also handle complex, non-linear data patterns well. Boosting can be sensitive to noisy data and may overfit if not properly regularized. Additionally, boosting models tend to be slower to train compared to other algorithms, such as Random Forest [59].

2.2.5 Support vector regression (SVR)

Support Vector Regression (SVR) is based on the concept of Support Vector Machines (SVM), which are typically used for classification tasks [60]. SVR seeks to find a hyperplane that best fits the data within a defined margin of error (ε). The goal is to minimize the prediction error while keeping the model complexity as low as possible. SVR performs well in high-dimensional spaces and is effective when the data has complex, non-linear relationships [61]. It is particularly useful when the dataset is small or the number of data points is few but significant. SVR is sensitive to the choice of the kernel and regularization parameters. It also does not scale well with extensive datasets and can become computationally expensive [62].

2.2.6 Extreme gradient boosting (XGB)

XGB is an optimized version of Gradient Boosting, designed for speed and performance. It utilizes a gradient boosting framework, incorporating regularization techniques to prevent overfitting and enhance model generalization. It also includes parallelization for faster training on large datasets. XGB is one of the most accurate and efficient machine learning algorithms, particularly well-suited for datasets with complex, non-linear relationships. It consistently performs well in predictive modeling competitions [63]. While XGB is powerful, it can be sensitive to parameter tuning and may require significant computational resources for training large models. It also has higher complexity compared to simpler models, such as Random Forest or KNN.

To prevent overfitting, several measures were employed during the development of the machine learning models. A 10-fold cross-validation technique was applied to all models to assess their generalizability. This method divides the dataset into 10 equal folds, using 9 for training and 1 for validation in each iteration. The model's performance is averaged across all 10 iterations, providing a reliable estimate of its predictive accuracy on unseen data. Monitoring of training and validation errors was carried out to detect signs of overfitting. In cases where the training error deviated significantly from the validation error, adjustments were made to prevent the model from overfitting to the training data. Additionally, hyperparameter tuning was conducted to optimize the models and prevent them from becoming overly complex. Regularization parameters for models such as Support Vector Regression (SVR) and Random Forest (RF) were fine-tuned to minimize the impact of noise in the data.

2.3 Performance indicators

To evaluate the performance of the machine learning models, we employed several key metrics: R², RMSE, MAE, SI, and a20 [64]. These indicators provide insight into how well each model predicts compressive strength and the extent of errors in the predictions.

2.3.1 Coefficient of determination (R^2)

R² measures the proportion of variance in the dependent variable (compressive strength) that is explained by the model and Eq. (1). It ranges from 0 to 1, with higher values indicating a better fit.

$$R^2 = \left(\frac{\sum_i \left(P_i - \bar{P}\right)\left(E_i - \bar{E}\right)}{\sqrt{\sum_i \left(P_i - \bar{P}\right)^2} \sqrt{\sum_i \left(E_i - \bar{E}\right)^2}} \right)^2 \tag{1}$$

where E_i is the observed value, P_i is the predicted value, $\bar{E}$ is the mean of the observed values, and $\bar{P}$ is the mean of the predicted values.

2.3.2 Root mean squared error (RMSE)

RMSE quantifies the average magnitude of errors between predicted and actual values, as calculated by Eq. (2). It is sensitive to significant errors, making it a suitable metric for evaluating model precision.

$$RMSE = \sqrt{\frac{\sum_{i=1}^{n} \left(E_i - P_i\right)^2}{N}} \tag{2}$$

where n is the number of observations.

2.3.3 Mean absolute error (MAE)

MAE measures the average of the absolute differences between predicted and actual values, as calculated by Eq. (3). Unlike RMSE, it is not sensitive to outliers and provides a straightforward interpretation of prediction error.

$$MAE = \frac{\sum_{i=1}^{n} \left(|E_i - P_i|\right)}{N} \tag{3}$$

2.3.4 Scatter index (SI)

SI assesses the consistency between predicted and actual values in terms of relative error, as calculated by Eq. (4). A lower SI indicates a model that provides more consistent predictions.

$$SI = \frac{RMSE}{\bar{E}} \tag{4}$$

2.3.5 Fraction of predictions within 20% error range (a20)

The a20 metric calculates the fraction of predictions that fall within 20% of the actual value, as calculated by Eq. (5). This indicator helps gauge the model's practical accuracy.

$$a20_{index} = \frac{N20}{N} \tag{5}$$

These performance indicators are used to evaluate the accuracy and reliability of the machine learning models, offering a comprehensive view of how well the models predict compressive strength.

2.3.6 Taylor diagram

In addition to the statistical performance indicator mentioned above, two graphical indicators —namely, the Taylor diagram and the error distribution graph —were also used to evaluate the accuracy of the machine learning models. The Taylor diagram is a powerful graphical tool that offers a comprehensive evaluation by simultaneously visualizing three key performance metrics: correlation, root mean squared error (RMSE), and standard deviation. The Taylor diagram constructs a visual representation of these metrics. The x-axis depicts centered RMSE, with lower values signifying better agreement. The y-axis represents the correlation coefficient, with higher values indicating stronger relationships. A reference point at the origin (centered RMSE of 0 and correlation of 1) symbolizes the perfect model performance. Each model being evaluated is represented by a distinct point on the diagram. The closer a model's point is to the reference point, the better its overall performance in correlation, RMSE, and capturing variability. A standard deviation arc centered on the reference point is also often included. This arc represents the variability observed in the actual data. Ideally, a model's point should lie on this arc, indicating it accurately reproduces the natural fluctuations present in the data.

2.3.7 Error distribution

An error distribution graph is a visual representation in machine learning that unveils how often specific error values occur within a model's predictions. It essentially depicts the distribution of discrepancies between predicted and actual target values. This graph offers valuable insights for evaluating model accuracy in multiple dimensions. The shape of the distribution itself can be informative. A symmetrical distribution centered around zero suggests minimal bias, indicating the model's predictions are neither systematically overestimating nor underestimating the actual values. Conversely, a skewed distribution in a particular direction suggests bias. A wider distribution signifies higher variance, implying the model's predictions exhibit greater scatter around the actual values.

3 Comparison code and empirical equation

Standard codes are beneficial for predicting the compressive strength of hollow block masonry. Codes do not directly indicate masonry strength; instead, they provide reduction factors based on factors such as masonry unit strength, mortar type (strength and joint thickness), and the dimensions of the prism or wallet. Table 2 summarizes the equations for the compressive strength of hollow block masonry, as proposed by the standard code and published literature. Eurocode 6 [38] provides the equation and tables for calculating the compressive strength of masonry, including hollow block masonry, as shown in Eq. (6). The K value depends on the masonry unit group and the type of mortar used. It considers factors like the presence of hollow cores when categorizing the masonry unit group. Although BS 5628 considers several factors, this approach is simplified and does not account for factors such as the geometry and net area of the hollow block, which can influence its strength. AS 3700 [65] uses Eq. (7) to determine the design compressive strength of masonry based on unit and mortar properties. It includes adjustment factors for the presence of hollow cores and the slenderness ratio of the masonry element. While AS 3700 offers a more sophisticated approach than Eurocode 6, it might not account for the unique properties of all types of hollow blocks. The design approach in AS 3700 relies on factors such as the height-to-thickness ratio and type of bedding, which can, in some cases, lead to an underestimate or overestimate of the strength of specific hollow block configurations. Both codes prioritize safety, which may result in calculated values lower than the achievable strength of some well-engineered hollow block assemblies.

Conversely, empirical equations rely on historical data and established relationships between block strength, mortar strength, and geometrical properties. Although several empirical equations are proposed for solid block masonry and grouted masonry, limited equations are available to predict the compressive strength of hollow block masonry. Based on three-dimensional finite element analyses, Köksal et al. [66] proposed Eq. (8) for the compressive strength of hollow block masonry prisms based on the compressive strength of the masonry unit and mortar. Sarhat and Sherwood [8] proposed Eq. (9) based on a dataset collected from the published literature. While empirical equations offer a simple approach, they are often based on averaged data and may not capture the complex interactions between all influencing factors. These equations may not account for influential factors, such as the net-to-gross area ratio of the hollow block and the aspect ratio (length-to-thickness ratio) of prisms, which can lead to inaccurate predictions.

To compare the performance of the machine learning (ML) models with traditional methods, the study applied two widely recognized code-based and empirical models: Eurocode 6 and AS3700. These models are commonly used to estimate the compressive strength of hollow block masonry based on material properties, such as the compressive strength of the masonry unit (f_b) and mortar (f_m), as

Table 2 Summary of equations for compressive strength of Hollow block masonry

Equation source	Equation	Equation No	Remarks
Eurocode 6 [38]	$f_{mp} = K f_b^{\alpha} f_m^{\beta}$	(6)	K, α and β are constant; f_b, f_m and f_{mp} are the mean compressive strengths of the masonry unit, mortar, and masonry.
AS 3700 [65]	$f_{mp} = K_h K_m f_b^{0.5}$	(7)	K_h is the factor that accounts for the ratio of the masonry unit height to the mortar bed joint thickness; K_m is a factor that accounts for the type of bedding use; f_b is the mean compressive strength of the masonry unit.
Köksal et al. [66]	$f_{mp} = 1.57 \ln(f_m) + 0.75 f_b$	(8)	f_b, f_m and f_{mp} are the mean compressive strengths of the masonry unit, mortar, and masonry.
Sarhat and Sherwood [8]	$f_{mp} = 0.886\, C_b C_h f_b^{0.750} f_m^{0.180}$ $C_h = \begin{cases} \frac{1}{1-0.05\left(5-\frac{h}{t}\right)} & \frac{h}{t} < 5 \\ 1 & \frac{h}{t} \geq 5 \end{cases}$	(9) (10)	C_b adjusts for the type of mortar bedding used. It is set to 1.0 for face shell bedding and 0.91 for full bedding; f_b, f_m and f_{mp} are the mean compressive strength of the masonry unit, mortar, and masonry; h is the height of the prism; t is the thickness of the prism.

well as geometric properties like the height-to-thickness ratio (*H*/*t*). For both Eurocode 6 and AS3700, the calculations were carried out using the parameters extracted from the dataset, including the compressive strengths of masonry units and mortars, as well as the appropriate adjustment factors. These calculations allowed us to compare the predictive accuracy of these traditional models with that of the machine learning models developed in this study.

Figures 6, 7 and 8 compare the performance of estimates provided by the Eurocode, AS3700 and Sarhat and Sherwood [8] for predicting compressive strength. Eurocode predictions showed an RMSE of 6.82 MPa, and 28% of the predictions fell within a 20% margin of error compared to the actual strength. AS3700 showed an RMSE of 10.19 MPa, and only 16% of the predictions fell within a 20% margin of error compared to the actual strength. This is a lower percentage compared to Eurocode, signifying that even fewer predictions are within a reasonable margin of error. Based on this analysis, Eurocode performs better than AS3700 for predicting compressive strength in this case. Eurocode shows a moderate correlation and reasonable error levels, while AS3700 exhibits a poor correlation and higher errors. The underestimation trend in both models might be due to safety considerations or limitations in the models themselves.

Building codes prioritize safety. The equations in these codes might intentionally underestimate the actual strength to ensure structures can withstand real-world loads with a built-in safety margin. Additionally, the equations likely rely on material properties that are averages or exhibit inherent variability. Real materials can be stronger than these averages, leading to higher experimental results. The equations might not account for every factor that influences strength. Complexities such as the geometry of the hollow core, manufacturing variations, or interactions between units and mortar can be challenging to model accurately. Studies suggest that Eurocode equations might better fit hollow masonry than AS3700, which might be more conservative [67].

Compared to Eurocode and AS3700 estimations, Sarhat and Sherwood [8] provide more accurate estimations for compressive strength. It shows a lower RMSE of 3.94 MPa, and 75% of the predictions fall within a 20% margin of error compared to the actual strength. The expression proposed by Sarhat and Sherwood [8] incorporated

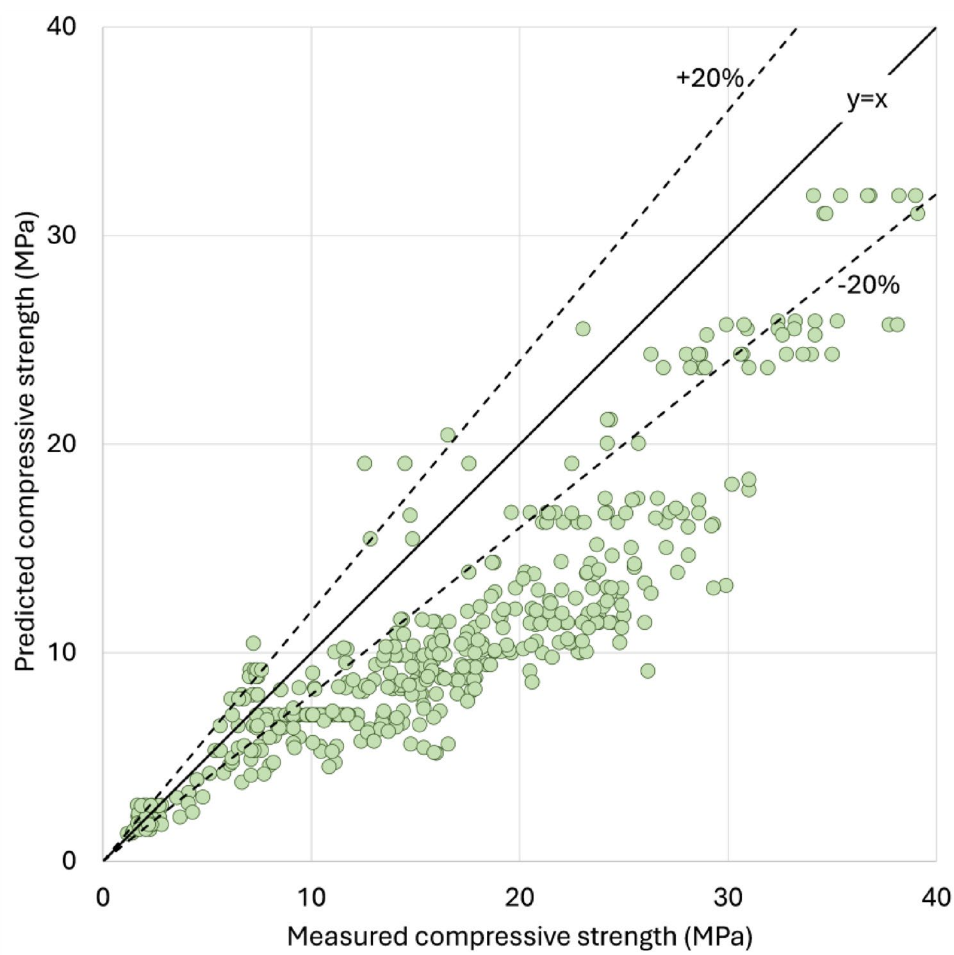

Fig. 6 Comparison between predicted value using Eurocode and actual value

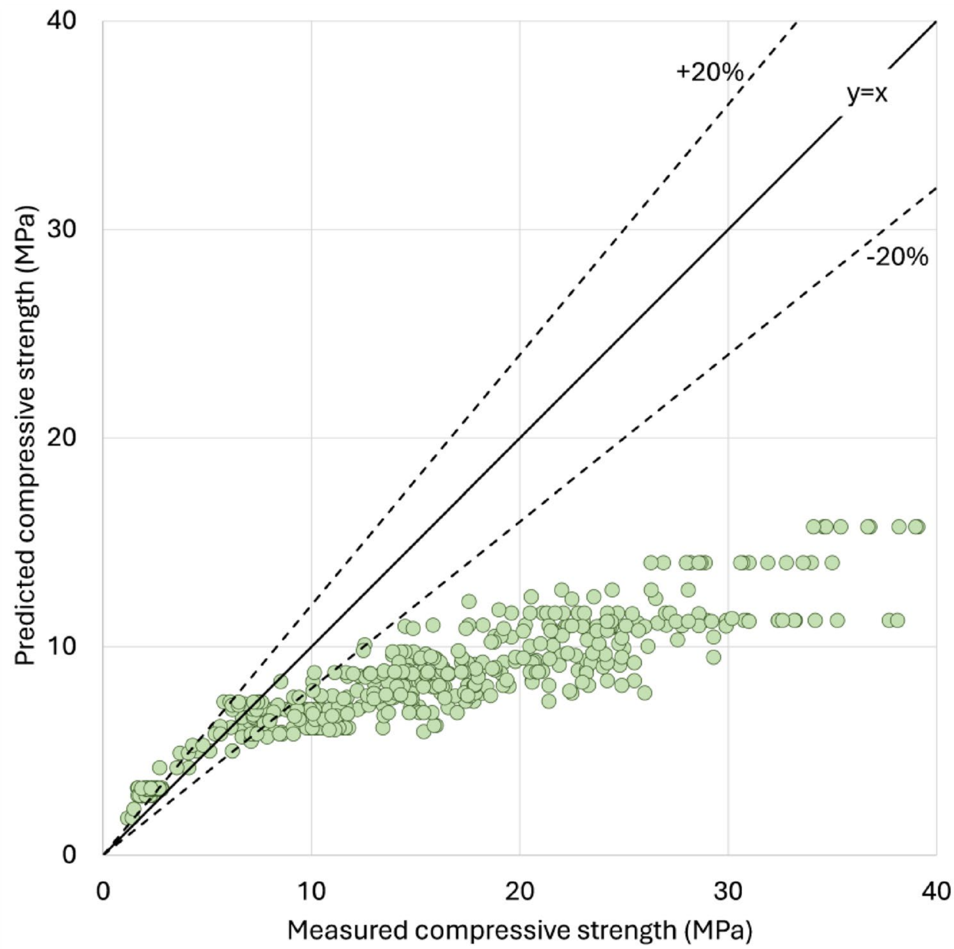

Fig. 7 Comparison between predicted value using AS3700 and actual value

the height-to-thickness ratio of the prism, which influences the estimation of compressive strength that Eurocode and AS3700 miss.

4 Results and discussion

4.1 Hyperparameter tuning

Table 3 details the hyperparameter tuning process for the machine learning models used in this study. Hyperparameters are crucial settings that influence how a model learns and performs. A grid search was conducted for both ANN and KNN to optimize the performance of each model, evaluating a range of possible values for each hyperparameter. For other models, a random search was conducted to optimize the hyperparameters. The table shows the model type, the hyperparameters explored, and the chosen value for each. For instance, the Artificial Neural Network (ANN) underwent a grid search for the number of hidden layers, nodes per layer, and learning rate. The optimal configuration for the ANN was two hidden layers with 13 nodes and a learning rate of 0.1. Similarly, hyperparameters such as the number of neighbors for K-Nearest Neighbors (KNN), the number of trees and splits per tree for Random Forest, and the kernel type and regularization parameters for Support Vector Regression (SVR) and XGB were optimized. This process ensured that each model was fine-tuned to achieve the best possible performance in predicting the compressive strength of hollow block masonry.

4.2 K-fold validation of the models

To rigorously evaluate the performance of the machine learning models and prevent overfitting, a ten-fold cross-validation technique was employed [68, 69]. This method provides a reliable estimate of a model's generalizability. The dataset was divided into ten equal folds, with each fold used once for validation and the remaining nine for iterative training, repeated ten times.

The effectiveness of cross-validation was assessed using R^2 and RMSE. As shown in Fig. 9, the XGB model outperformed the others, exhibiting superior R^2 and lower RMSE values for both training and validation datasets. Notably, all models except KNN and RF achieved an R^2 exceeding 0.92 for all folds. While training, R^2 values varied minimally

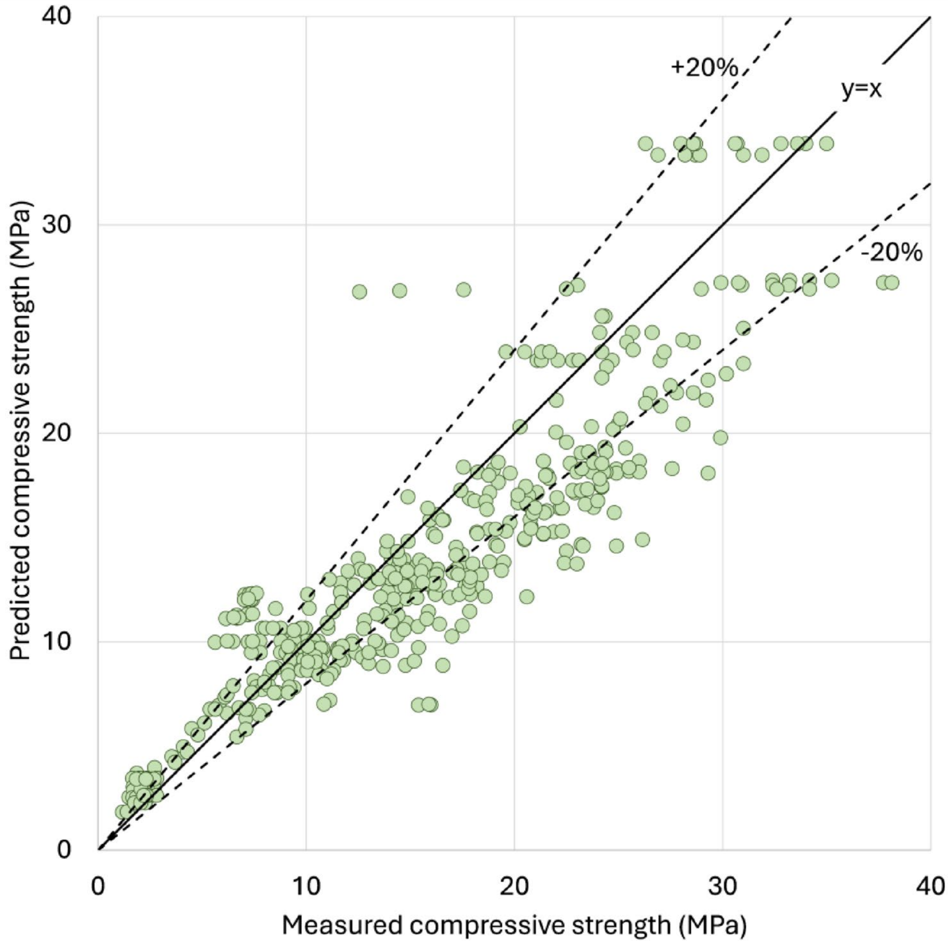

Fig. 8 Comparison between predicted value using the expression proposed by Sarhat and Sherwood [8] and actual value

across all models, only XGB showed similarly low variation (0.039) in validation R^2. This pattern was consistent with RMSE values. XGB demonstrated exceptional performance, with training RMSE ranging from 1.05 to 1.12 MPa and validation RMSE from 2.01 to 2.14 MPa. These results indicate that the models, particularly XGB, are robust against overfitting and reliable for prediction.

4.3 Performance of the machine learning models

When evaluating various machine learning models for predicting a specific outcome (f_{mp}), most demonstrated satisfactory performance, with the RF model being an exception (as shown in Fig. 10; Table 4). It is important to note the difference in methodology used to evaluate the performance metrics for the standard code equations and the machine learning models. The metrics for the standard code equations are based on a deterministic evaluation of the entire dataset, as these equations are not trained or optimized. In contrast, the performance metrics for the machine learning models (Random Forest, SVM, etc.) were calculated using an independent test dataset of 383 samples, which was not used during the training phase. Training dataset consists of 128 samples. The metrics presented for the standard code equations and empirical model in the Table 4 are based on entire dataset of 511 sample. Among the models tested, the XGB proved to be the most effective and reliable. This conclusion is supported by the XGB's significantly higher R^2 value compared to the other models. Furthermore, the XGB exhibited notably lower RMSE and MAE, indicating a strong ability to produce predictions that closely match observed data.

Additional analysis using metrics such as the SI and the a20 index reinforced the XGB's robustness. The lower SI values for the XGB (0.07 for training and 0.12 for testing) suggest its ability to minimize the difference between predicted and actual values. The a20 index showed that 97% of predictions for the training data and 92% of predictions for the testing data fell within a 20% error range. While other models, excluding the RF model, also showed reasonable performance (with over 84% and 76% accuracy within a 20% error range for training and testing data, respectively), the XGB model consistently outperformed them. These results indicate that the XGB model effectively captures complex relationships within the data, leading to superior

Table 3 Hyperparameters used for the machine learning models

Model	Hyperparameters	Analyzed Values	Selected value
Artificial Neural Network	Number of layers	[1, 2]	2
	Nodes per layer	[1–16]	13
	Learning rate	[0.01, 0.05, 0.1, 0.5, 1.0]	0.1
KNN	k	[1–10]	3
Boosted Tree	Number of layers	[1,10]	10
	Splits per tree	[1,50]	50
	Learning rate	[0.05,0.5]	0.4
	Minimum size split	[1,10]	3
	Row sampling rate	[0.1,0.5]	0.5
	Column sampling rate	1	1
Random Forest	Number of trees in the	[1–50]	13
	forest	[1, 3]	2
	Number of terms	[0.1,1]	0.75
	sampled per split	[1,10]	5
	Bootstrap sample rate	10	10
	Minimum splits per tree	[1,5]	3
	Maximum splits per tree		
	Minimum size split		
Support Vector Regression	Kernel	[linear, Radial basis function]	Radial basis function
	Cost	[0.01-5]	0.8719
	Gamma	[0.001-0.5]	0.6421
XGB	Max_depth	[1–5]	3
	Subsample	[0.5-1]	0.9472
	Colsample_by tree	[0.5-1]	0.8622
	Min_child_weight	[1–3]	1.1895
	Alpha	[0-0.5]	0.1998
	Lambda	[0–2]	1.1562
	Learning rate	[0.05–0.2]	0.1954
	Iterations	[0–40]	39

predictive accuracy. Its reliability and robustness position it as a valuable tool for forecasting and predictive analytics.

Taylor diagrams were applied to compare the performance of various machine-learning models. In the Taylor diagram, the correlation coefficient (R) and standard deviation (SD) are used to assess the model's effectiveness on both the training and testing datasets [70]. The Taylor diagram serves as a valuable visual tool, consolidating these two critical metrics into a single plot, as shown in Fig. 11. A point on the diagram represents each model. The distance from the reference (marked "Obs") reflects the model's SD. Concentric circles around the origin represent different correlation values, with points closer to the outermost circle indicating a stronger linear relationship between predicted and observed values. The ideal scenario positions a model on the circle with the highest correlation and at a radial distance from the origin equal to the standard deviation (SD) of the observed data.

The analysis yielded insights into the strengths and weaknesses of different models. XGB generally exhibited the highest correlation coefficients across both training and testing data. However, its SD on the testing data might be slightly higher than the observed data, suggesting potential overfitting. The SVR model demonstrated a significant reduction in SD compared to other models on the training data, indicating good generalization. However, its testing data correlation was lower than XGB, suggesting it might struggle with unseen data. Random Forest (RF) displayed the lowest correlation in both datasets and a lower SD on the training data, potentially signifying the underfitting of the data. The selection of the optimal model hinges on the specific application's priorities. If a robust linear relationship is paramount, XGB might be the preferred choice, but with caution regarding the risk of overfitting. For superior generalization, SVR shows promise, but its testing correlation should be carefully evaluated to ensure it meets the project's requirements. Models like BT or ANN might offer a balance between correlation and generalization, depending on their specific placement on the Taylor diagram.

Figure 12 illustrates the prediction error for various machine learning models. The analysis revealed that XGB emerged as the strongest performer based on prediction error. XGB exhibited the lowest average error in both the training dataset (−0.01) and the testing dataset (0.22), indicating its ability to make consistently accurate predictions. Additionally, XGB displayed a balanced distribution of errors, which is evident from its low skew values in both datasets. While a trend of a slightly increased average error was observed in the testing data compared to the training data across all models, this is a common and expected behavior for models that generalize effectively. The broader range of errors in the testing data simply suggests a greater variability in predictions for unseen examples, but does not indicate a significant issue with generalization.

4.4 Sensitivity analysis

SHAP (SHapley Additive exPlanations) analysis was employed to investigate the influence of various input variables on the predicted compressive strength of hollow block masonry. As XGB performed better compared to other models in predicting f_{mp}, the XGB model was used for the SHAP analysis. The obtained mean SHAP values, shown in Fig. 13 for each variable, provide insights into their contributions to the model's prediction. This figure shows the results of a SHAP sensitivity analysis for the XGBoost model, illustrating the contribution of each feature to the model's predictions.A high SHAP value for f_b signifies that the model heavily considers the compressive strength of the masonry units when predicting the overall strength. Intuitively, stronger bricks lead to a more robust structure and a higher predicted compressive strength. The moderately positive SHAP value for f_m indicates that mortar strength also plays a role, but to a lesser extent than the bricks themselves.

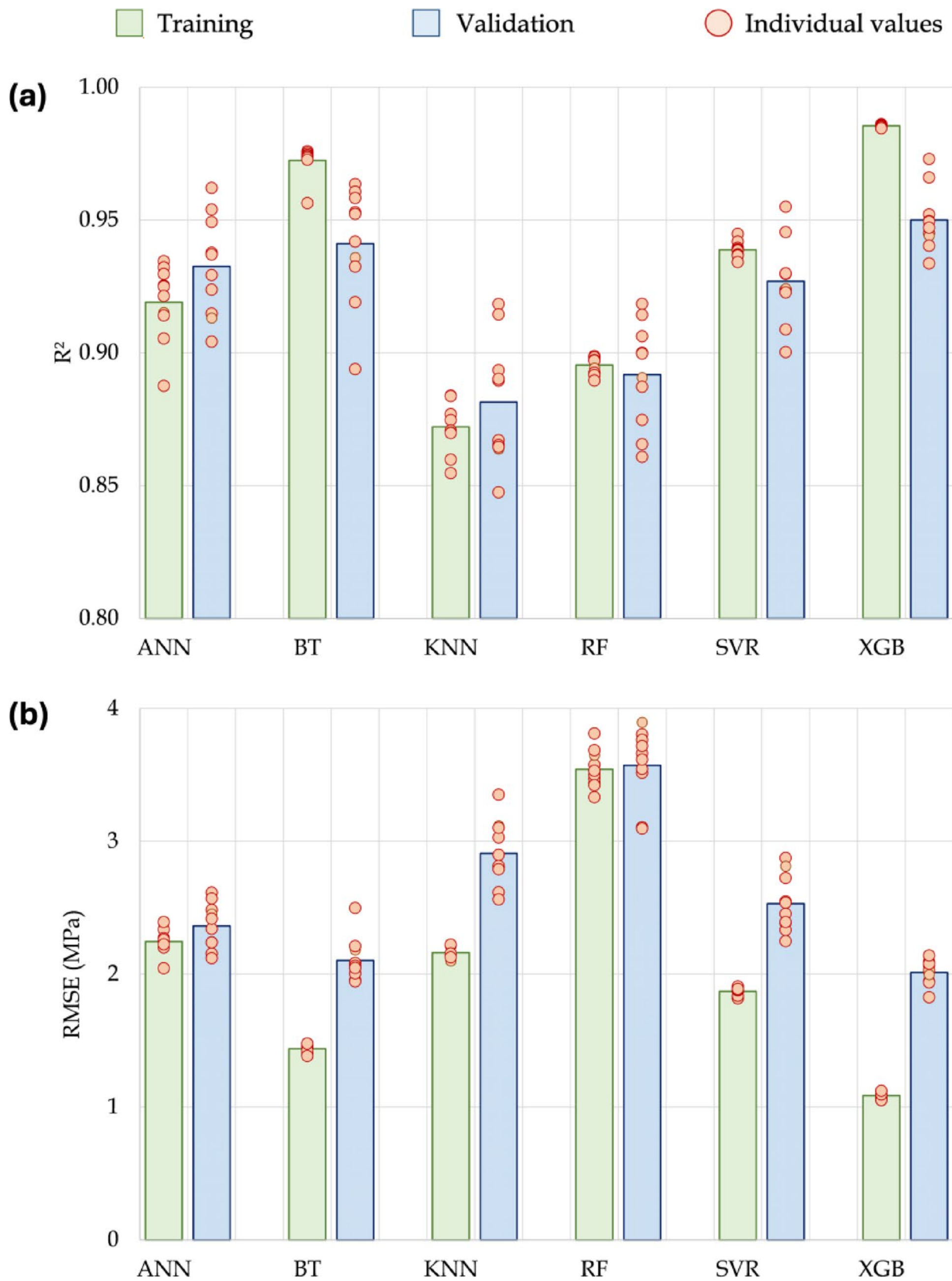

Fig. 9 Performance indicators for K-fold validation (a) R^2 and (b) RMSE

Stronger mortar contributes to a better bond between bricks, enhancing the structure's capacity to withstand compressive forces. The influence of H/t, L/t, α, t_m and bedding type is less pronounced than the abovementioned factors. The mean SHAP values provide a general overview and further investigation into individual data points, and their corresponding SHAP values can reveal intricate interactions between these factors and their influence on the model's predictions in various scenarios.

To enhance the interpretability of machine learning models, beeswarm SHAP graphs offer a compelling visualization technique. They go beyond traditional sensitivity analysis measures by revealing how individual features influence model predictions for each data point. The beeswarm plot displays features on the y-axis and SHAP values on the x-axis, as shown in Fig. 14. SHAP values depict a feature's contribution to a prediction, with positive values indicating a push towards the positive class and negative values signifying a push towards the negative class. A dot represents each data point, and its color corresponds to the specific value of the corresponding feature (e.g., red for high values, blue for low values).

The results show that both f_b and f_m have a positive impact on f_{mp}. A wider spread of dots on the x-axis for f_b signifies a

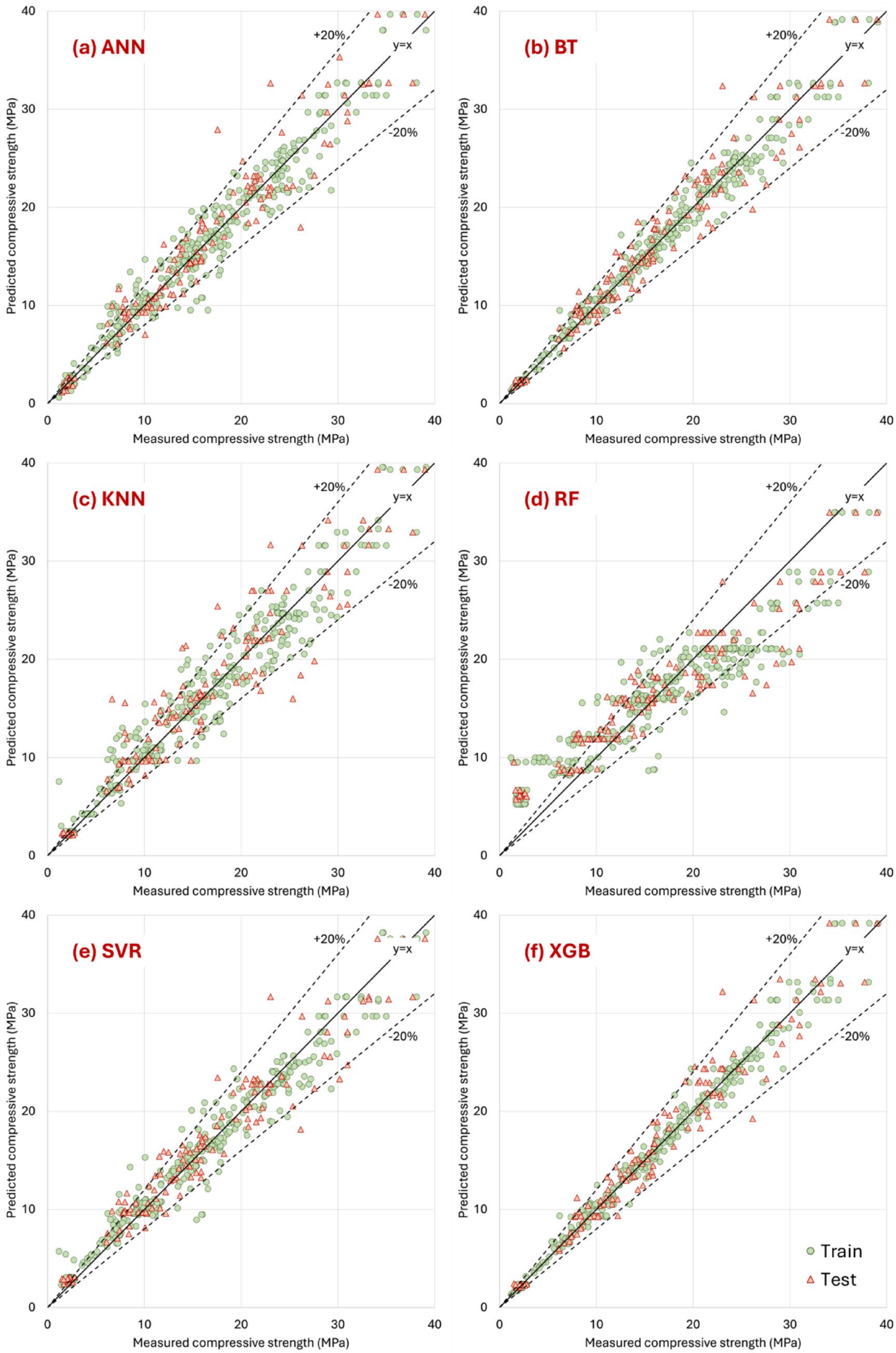

Fig. 10 Predicted vs. actual compressive strength for various machine learning models (**a**) ANN, (**b**) BT, (**c**) KNN, (**d**) RF, (**e**) SVR and (**f**) XGB

Table 4 Performance indicator for different codes, empirical model, and machine learning models

Code/Model	Description	Train					Test				
		R^2	RMSE (MPa)	MAE (MPa)	SI	a20	R^2	RMSE (MPa)	MAE (MPa)	SI	a20
Code [1]	Eurocode	0.44	6.82	5.64	0.42	0.28					
	AS 3700	0.25	10.19	7.98	0.63	0.16					
Empirical model [1]	Sarhat and Sherwood	0.81	3.94	3.03	0.24	0.75					
ML model	ANN	0.95	1.91	1.39	0.12	0.86	0.94	2.43	1.70	0.15	0.84
	BT	0.98	1.37	0.94	0.09	0.96	0.95	2.22	1.59	0.13	0.89
	KNN	0.94	2.15	1.54	0.13	0.84	0.89	3.15	2.21	0.19	0.76
	RF	0.90	3.61	2.88	0.22	0.61	0.89	3.74	2.91	0.22	0.63
	SVR	0.96	1.87	1.34	0.12	0.85	0.94	2.42	1.76	0.15	0.77
	XGB	0.98	1.17	0.72	0.07	0.97	0.95	2.06	1.44	0.12	0.92

[1]The metrics for the standard code equations and empirical model are based on a deterministic evaluation of the entire dataset

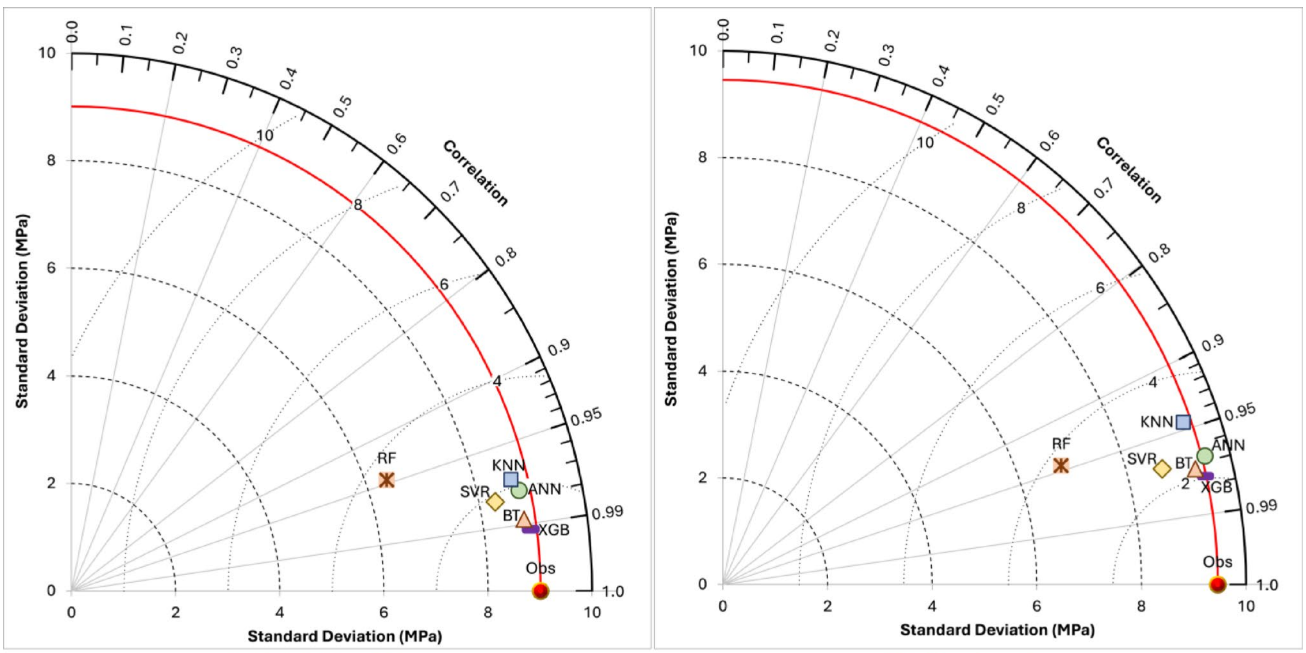

(a) Training dataset (b) Testing dataset

Fig. 11 Taylor diagram for (**a**) training dataset and (**b**) testing dataset

more significant impact on the f_{mp}. Stronger hollow blocks can withstand higher compressive loads before failure [50]. The block's net area (solid area) directly contributes to the overall strength of the prism [40]. Mortar plays a crucial role in transferring load between the blocks. While stronger mortar can somewhat improve the overall strength, its influence is often less pronounced than the block strength. Mortar joints are typically much thinner than the block itself. This limits the contribution of mortar strength to the overall strength of the composite. Even with weaker mortar, the interlocking of blocks and the confining effect of the mortar on the block faces can provide significant strength [67].

When the slenderness effect was considered, both H/t and L/t ratios negatively affected the f_{mp}. As the H/t ratio increases (taller and thinner prisms), the structure becomes slender and more prone to buckling under compression. This can decrease the overall compressive strength compared to a shorter and thicker prism made of the same materials [71]. The L/t ratio generally has a less significant impact on compressive strength than the H/t ratio. This is because the load is primarily transferred through the vertical axis of the prism (height) during compression. However, for very long and thin prisms (high L/t), there is a possibility of shear failure along the mortar joints. This can become a concern if the L/t ratio is substantial [72]. Building codes and standards often specify recommended H/t ratios for testing hollow masonry prisms to ensure accurate strength evaluation. In practice, a balance must be struck. While lower h/t ratios may offer higher strength, they might be less efficient for wall construction due to increased material usage [7].

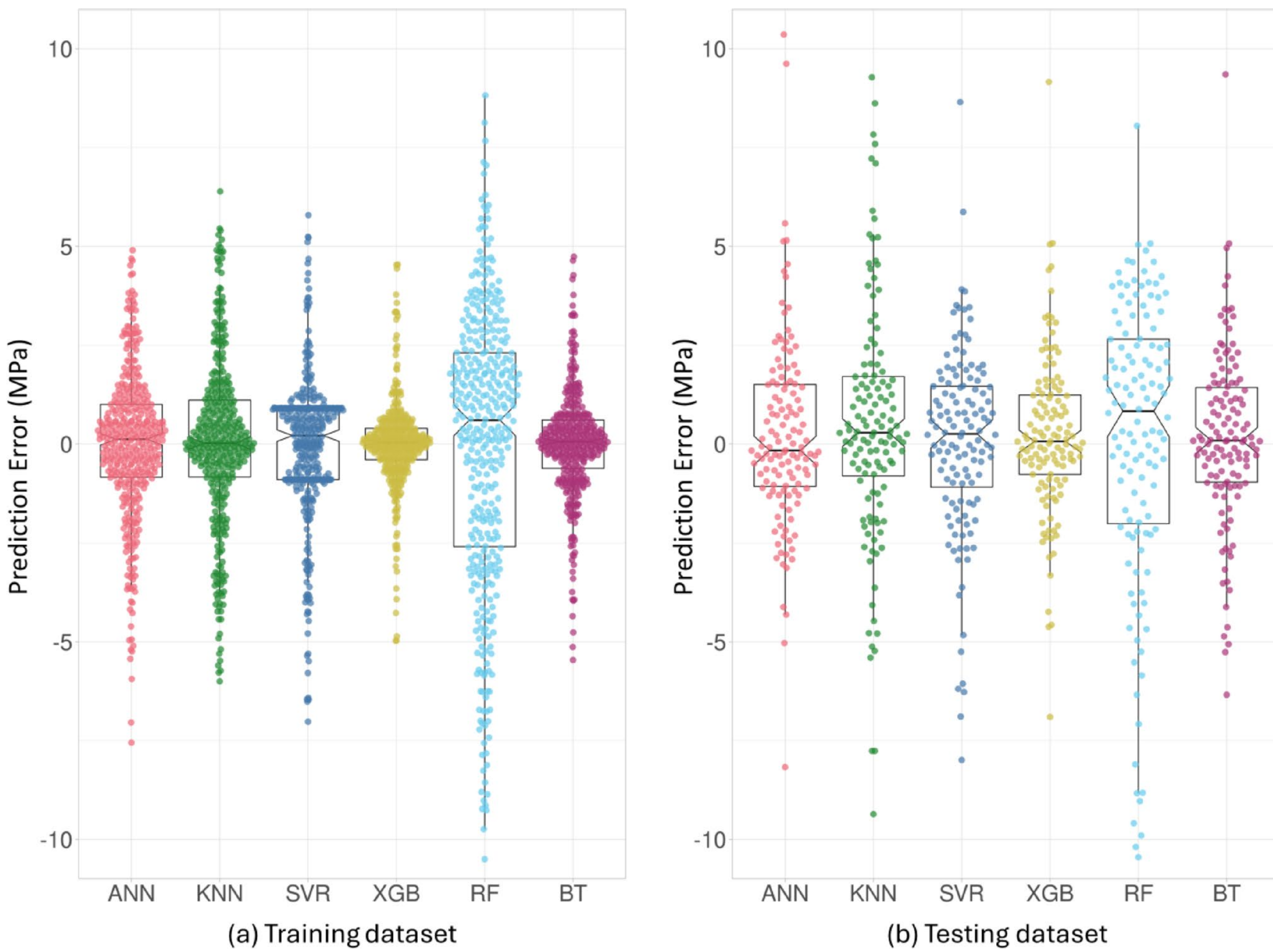

Fig. 12 Prediction error distribution for various machine learning models (a) training dataset and (b) testing datasets

Fig. 13 Mean SHAP value for the various input variables using XGB model

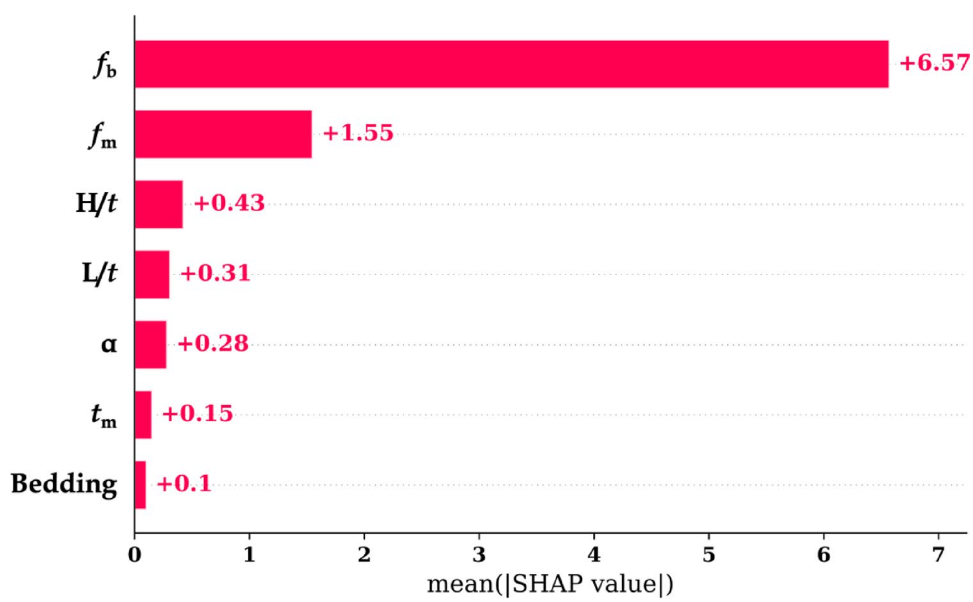

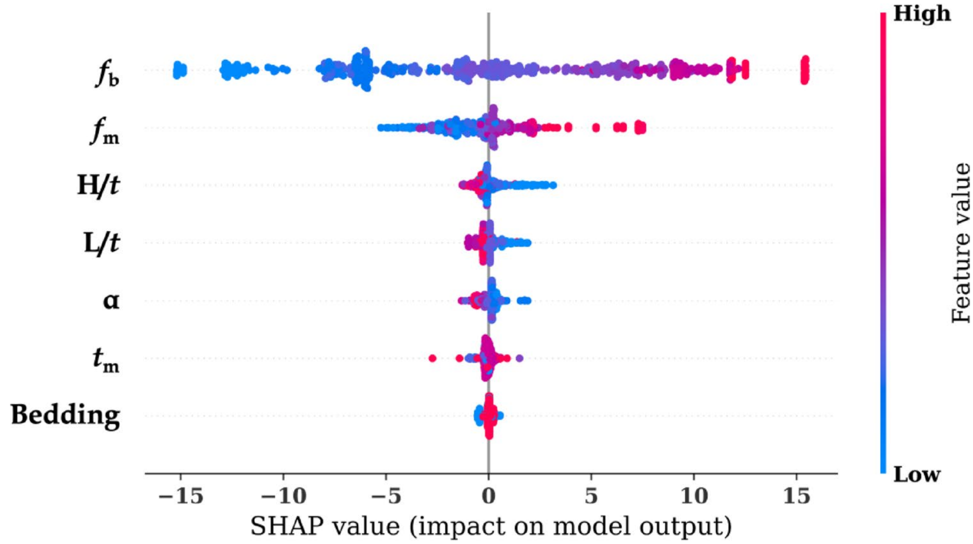

Fig. 14 A beeswarm SHAP graph for various input variables using XGB model

Both the net-to-gross area of hollow blocks (α) and mortar thickness have a complex relationship with f_{mp}. In the study, fb is considered net area compressive strength; the individual effect of α is complicated to interpret. Similarly, the thickness of the mortar joint in hollow masonry prisms has a complex relationship with the compressive strength. It can have a positive impact, but to a lesser extent than the strength of the hollow blocks. Thicker mortar joints can provide a larger area for contact between the blocks. This allows for better distribution of compressive loads across the entire block surface, potentially leading to a slight increase in overall strength [73]. A thicker mortar layer can help bridge minor imperfections on the block surfaces, creating a more uniform load distribution and potentially mitigating stress concentrations that could lead to premature failure. The mortar joint typically represents a much smaller area than the solid block. Even with a thicker joint, the strength of the mortar is often lower than the block material [74]. Therefore, the increase in strength due to thicker mortar is usually modest. Excessively thick mortar joints can have negative consequences, such as using less block material within the prism, which potentially reduces its overall load-bearing capacity.

Figure 15 illustrates how various block features impact the predicted f_{mp}. While strong fb and mortar generally lead to stronger prisms, this is not always true. In most cases, strong f_b influences f_{mp} more than strong mortar. Figures 15(b) and 15(c) focus on the influence of the solid part of blocks (α) and prism aspect ratios (H/t and L/t). They reveal that only prisms with low H/t and L/t ratios tend to use blocks with low α. For prisms with H/t ratios exceeding 5.0, blocks with higher solid portions ($\alpha > 0.60$) are generally preferred. Interestingly, blocks with less void ($\alpha > 0.60$) used in high H/t ratio prisms have negative SHAP values. This implies that the H/t ratio has a more substantial influence on f_{mp} than the α in such cases. A similar trend is observed for the L/t ratio, suggesting that the prism's aspect ratio plays a more significant role in f_{mp} than the block's α value for specific geometries.

4.4.1 Relative compressive strength of masonry unit and mortar on sensitivity analysis

The ratio between the f_m and f_b significantly impacts the structure's overall strength. A higher f_m/f_b ratio typically translates to stronger masonry. This is because the mortar can bind the individual units more efficiently, creating a more cohesive structure. Conversely, a lower f_m/f_b ratio can lead to weaker masonry as the mortar's bonding ability is compromised. To investigate the effect of these, the influence of block strength relative to mortar strength on the prediction accuracy of compressive strength for hollow masonry blocks was examined. From the dataset used in the present study, it is found that in 357 cases, the f_b was higher than f_m. The opposite was true in the remaining 154 cases, with f_b being lower than f_m.

Data were analyzed for both the training and testing datasets under these two scenarios ($f_b > f_m$ and $f_b < f_m$), and the results are illustrated in Fig. 16(a). In both scenarios, the training datasets achieved excellent performance with R^2 values close to 0.98 and a high percentage of data points falling within the 20% error range. This indicates that the model effectively learned the relationship between the input parameters and compressive strength in the training data. While the training data showed high accuracy, the testing data for the scenario where f_b is greater than f_m exhibited decreased performance. This is evident from the lower R^2 (0.93) and a reduced fraction of data points within the 20% error range (0.96) compared to the training data. Interestingly, the testing data for the scenario where f_b is less than

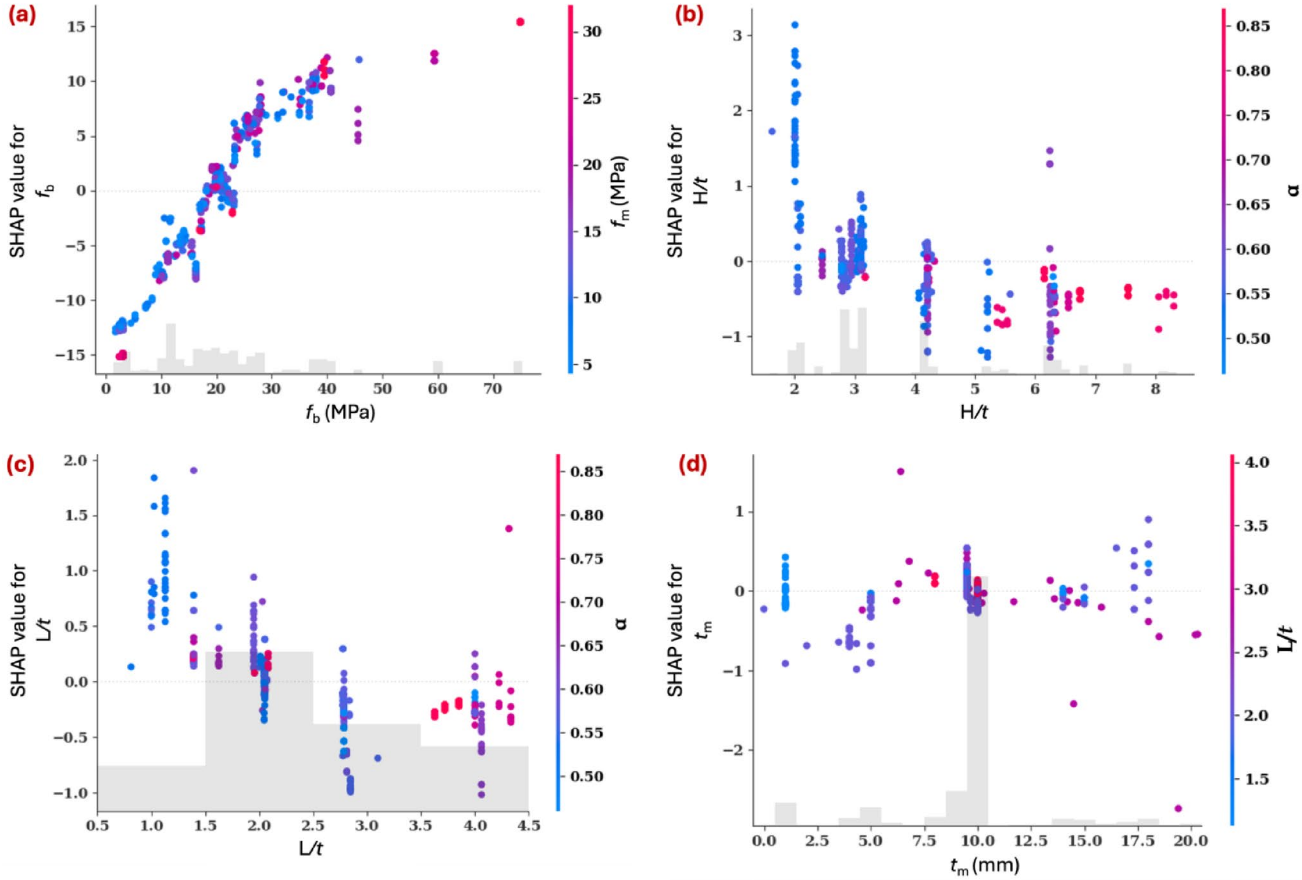

Fig. 15 Partial dependence plot from SHAP analysis

f_m maintained a high accuracy comparable to the training data. The R^2 value remained close to 0.98, and the fraction of data points within the 20% error line remained respectable at 0.84, although this was significantly lower than the training dataset.

As shown in Fig. 16(b), the SHAP analysis reveals that the relative influence of input variables depends on the relationship between the f_b and f_m. In cases where the f_b is greater than the f_m, the SHAP values indicate that the f_b exerts the most decisive influence on the overall compressive strength. This is intuitive, as stronger blocks naturally contribute to more robust structures. The compressive strength of the mortar remains important but has a lower impact than the block strength. Geometric features, including the L/*t*, H/*t*, and t_m, all contribute moderately to the final compressive strength. The α, representing the ratio of solid area to total area, also has a moderate influence. Finally, the type of bedding used has a minor impact on the overall compressive strength. However, the scenario changes significantly when f_b is lower than f_m. While the f_b remains the most critical factor, its influence weakens slightly compared to the $f_b > f_m$ case. This suggests that even weaker blocks can contribute meaningfully, albeit to a lesser extent. Interestingly, the importance of mortar strength diminishes when the block is weaker, highlighting its role in compensating for deficiencies in block strength. In such cases, optimizing factors like bedding type becomes crucial to maximize the mortar's contribution to the overall strength. Additionally, the influence of geometrical features becomes minimal. This suggests that when the block is the weak link, the overall geometry becomes less critical in determining the final compressive strength.

4.4.2 Effect of prism height on sensitivity analysis

The specimen's height is another factor affecting the masonry prism's compressive strength. Generally, taller and thinner prisms tend to be weaker than shorter and thicker ones under compressive loads. The dataset used in the present study shows that in 307 cases; the H/*t* ratio is less than 4. In the remaining 204 cases, the H/*t* ratio is higher than 4. This criterion is critical for ensuring that the observed failure mode is a result of compressive crushing of the masonry rather than premature failure caused by lateral instability or buckling of the slender prism. This geometric limit is consistent with established design standards. For example,

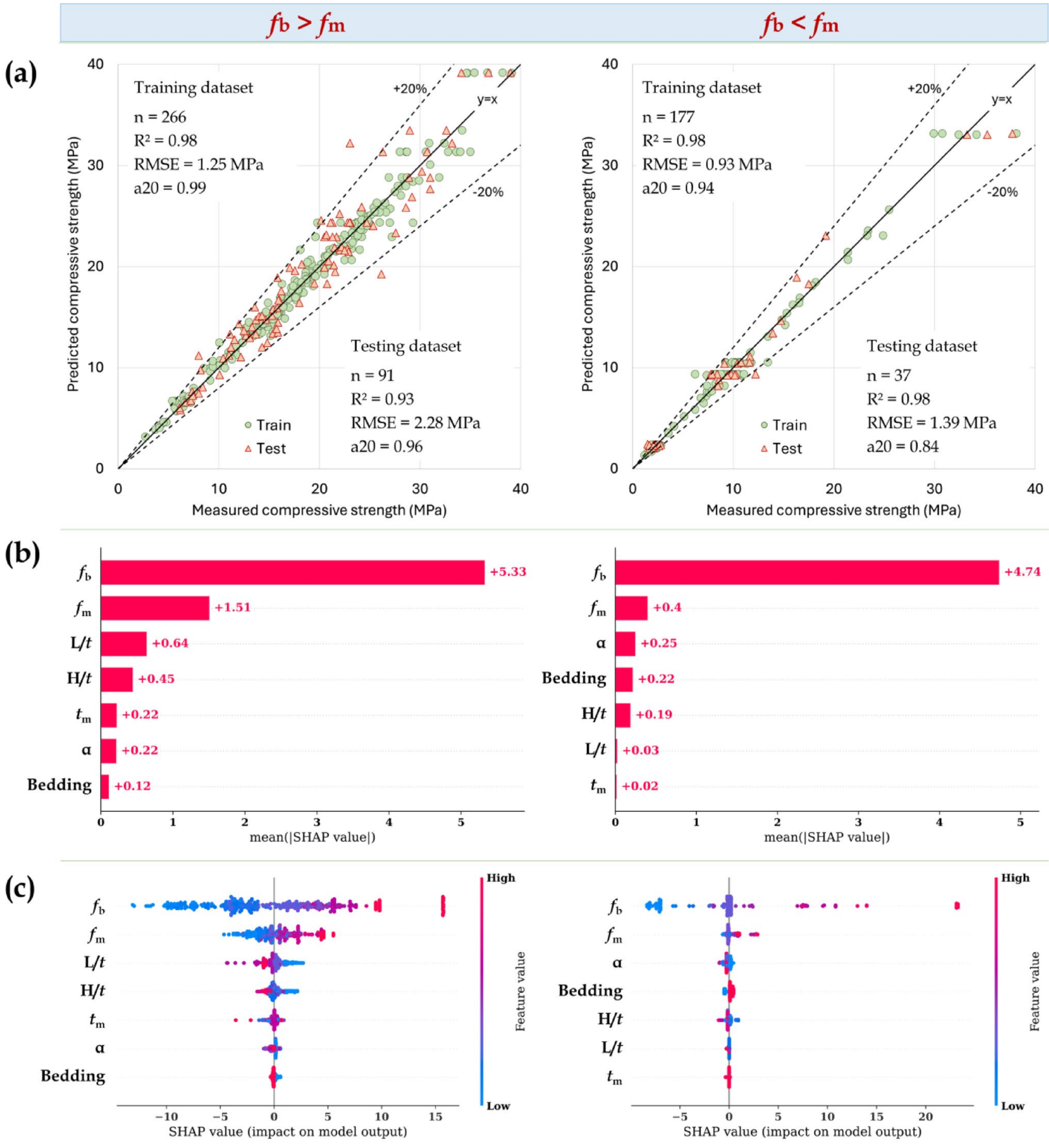

Fig. 16 Effect of prism height on sensitivity analysis (**a**) Predicted vs. measured compressive strength, (**b**) Mean SHAP value and (**c**) SHAP summary plot

Eurocode 6 (EN 1996-1-1) and other international standards specify similar slenderness ratios for compression testing to obtain reliable strength data. Prisms with a higher H/t ratio consistently exhibit a lower compressive strength due to buckling effects, which highlights the necessity of controlling this parameter in experimental studies. Therefore, selection of prisms with an H/t ratio less than 4 aligns with established best practices for obtaining representative material properties. Data were analyzed for both training and testing datasets under these two scenarios (and results illustrated in Fig. 17(a).

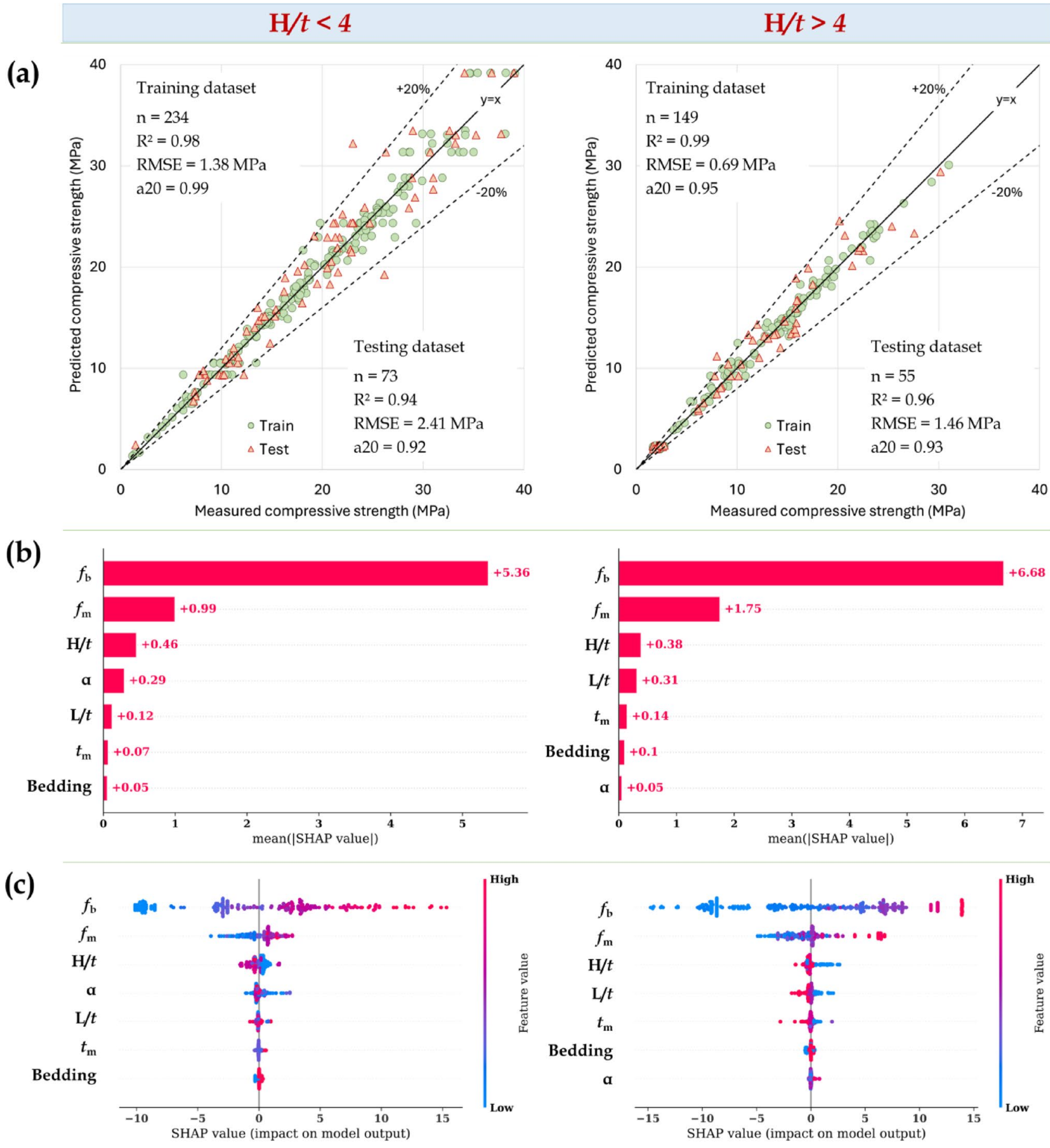

Fig. 17 Effect of prism height on sensitivity analysis (**a**) Predicted vs. measured compressive strength, (**b**) Mean SHAP value, and (**c**) SHAP summary plot

For shorter prisms (H/t<4), the model exhibited exceptional performance in predicting compressive strength. This is evidenced by the high R^2 values (0.98 for training and 0.94 for testing), indicating a strong correlation between predicted and actual strengths. The low RMSE values (1.38 for training and 2.41 for testing) demonstrate high model accuracy. Furthermore, the high fraction of data points falling within a 20% error range of the actual values (0.99 for training and 0.92 for testing) signifies excellent model generalizability. While the model's performance remained excellent for taller prisms (H/t>4), it was slightly lower than for shorter ones. The R-squared values (0.99 for training and 0.96 for testing) remained high, indicating a strong relationship between predicted and actual strengths. The training set exhibited a lower RMSE (0.69) than shorter prisms, suggesting better accuracy for this category during training. However, the testing set RMSE (1.46) was slightly higher. The fraction within the 20% error range also remained high (0.95 for training and 0.93 for testing), indicating good generalizability. This observed trend suggests that the model performs marginally better for predicting the compressive strength of shorter masonry prisms. This could be attributed to two potential factors. Firstly, shorter prisms experience a more uniform stress distribution under compression than taller ones. This simpler stress pattern might be more straightforward for the model to capture accurately. Secondly, failure modes in shorter prisms are more likely due to the crushing of units or mortar joints, which the model may be better at predicting compared to buckling failures that can occur in taller prisms.

As shown in Fig. 17(b), the SHAP analysis results revealed a noteworthy trend in how feature sensitivity is affected by this geometric factor. For shorter prisms ($H/t<4$), the f_b itself emerges as the most critical factor (SHAP: 5.34), unsurprisingly highlighting the dominance of block strength in determining overall strength. The f_m (SHAP: 0.99) also plays a significant role, but to a lesser extent. Interestingly, the H/t ratio has a moderate impact on predicted strength (SHAP: 0.46) for shorter prisms. This suggests that within this range, the effect of variations in height is less pronounced. Similarly, the L/t ratio (SHAP: 0.32) exerts a moderate influence, indicating that the overall aspect ratio contributes to strength prediction for shorter prisms. Other features, such as α (0.29), t_m (0.07), and bedding type (0.05), have a minor influence on the predicted strength for shorter prisms.

However, the trend in feature importance shifts for taller prisms ($H/t>4$). The f_b remains the most crucial factor (SHAP: 6.68), but its importance increases compared to shorter prisms. This could be attributed to the greater susceptibility of taller prisms to weaknesses in the block material. The importance of f_m (SHAP: 1.75) also increases, suggesting that a stronger mortar becomes more critical in compensating for potential deficiencies in the block for taller and potentially weaker structures. The H/t ratio (SHAP: 0.38) remains moderately essential, but its influence is slightly lower than shorter prisms. This might indicate a diminishing effect of height variation within the taller category. The impact of L/t ratio (SHAP: 0.31) also shows a slight decrease compared to shorter prisms. Notably, the importance of α (0.05) and t_m (0.14) decreases for taller prisms. The type of bedding (0.01) has minimal influence. This suggests that for taller structures, the focus shifts towards the overall strength of the block material and the mortar's ability to compensate, with less emphasis on these other factors. This emphasizes the dominance of block strength and highlights the increasing role of mortar strength, as well as a moderate influence of geometry, particularly for taller prisms.

4.4.3 Effect of bedding type on sensitivity analysis

Bedding type significantly impacts hollow block masonry's compressive strength. Full bedding utilizes more mortar, distributing compression load evenly but introducing potential weak points. Faceshell bedding, which uses mortar only on block faces, offers faster construction and a more defined load path, but may be less resistant to shear forces. The dataset used in the present study revealed that in 379 cases, the prisms were used with full bedding. In the remaining 132 cases, the prisms used the faceshell bedding. Data were analyzed for both training and testing datasets under these two scenarios (and results illustrated in Fig. 18(a).

The model consistently achieved superior performance when predicting the compressive strength with faceshell bedding compared to full bedding. This was evident in all performance metrics. For faceshell bedding, the model achieved a higher training and testing R^2 (closer to 0.99), indicating a stronger correlation between predicted and actual values. Additionally, the model produced lower prediction errors (lower RMSE values, around 0.75 for training and 1.89 for testing) for faceshell bedding compared to full bedding (around 1.28 for training and 2.11 for testing). Finally, the model captured a more significant portion of data points within a 20% error margin for faceshell data (around 98% for training and 90% for testing) compared to full bedding (around 97% for training and 93% for testing). Several potential explanations could account for this observed trend. Faceshell bedding typically involves less mortar compared to full bedding. This might lead to a more predictable load transfer path between the blocks. A simpler load transfer mechanism could enable the model to learn the relationship between input features and compressive strength more effectively. Additionally, faceshell bedding might introduce less overall variability in the masonry's behavior compared to full bedding. This reduced variability could make it easier for the model to identify the underlying patterns and achieve higher accuracy in its predictions. Furthermore, the distribution of compressive strength data for faceshell bedding might align more with the model's assumptions. This could contribute to better training and generalization of unseen data during testing.

As shown in Fig. 18(b), the SHAP analysis results revealed a noticeable difference in the importance of various features depending on the bedding type used. The analysis revealed a significantly higher SHAP value for the full bedding scenario (7.21) compared to the faceshell

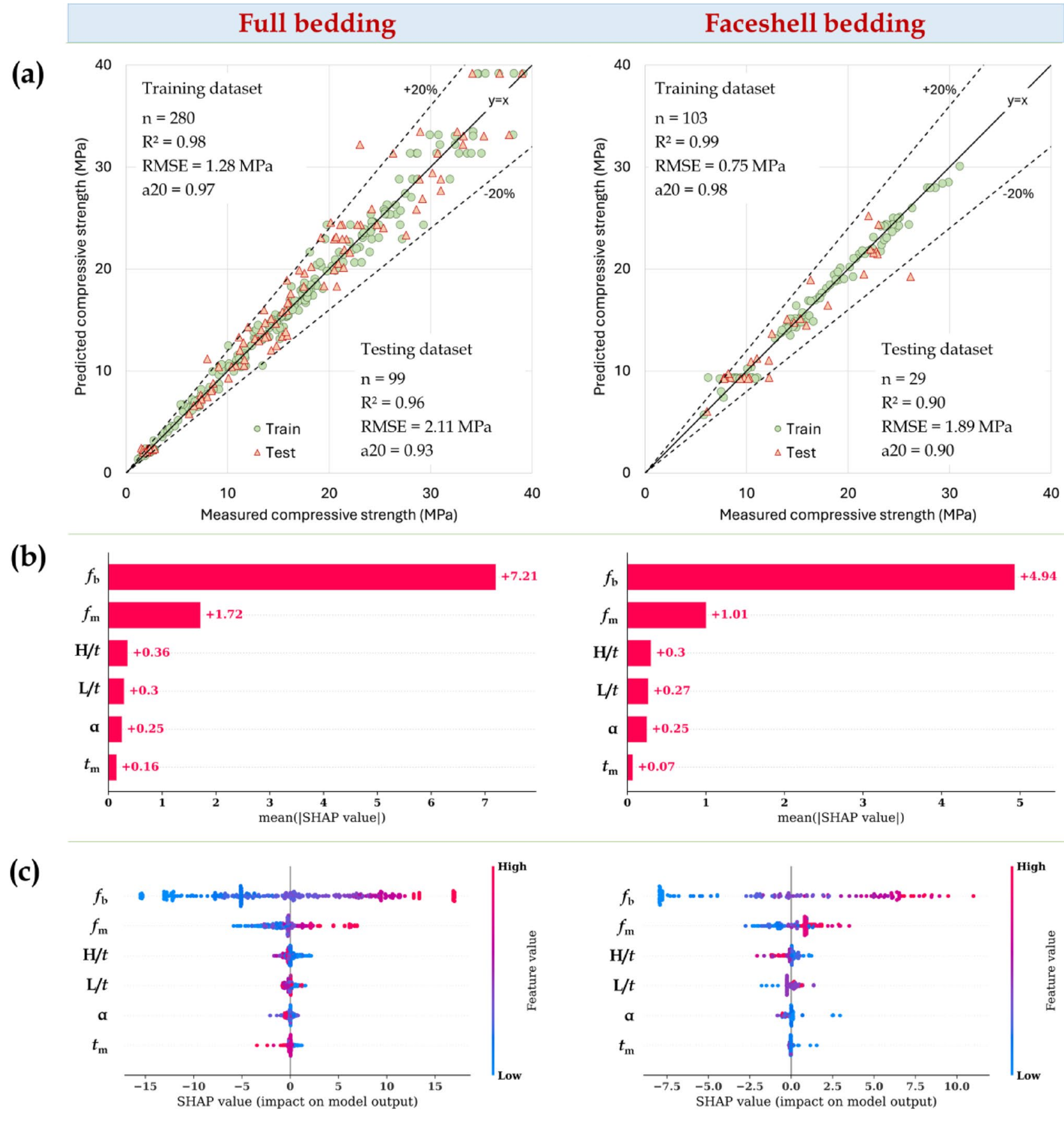

Fig. 18 Effect of bedding type on sensitivity analysis (**a**) Predicted vs. measured compressive strength, (**b**) Mean SHAP value, and (**c**) SHAP summary plot

bedding scenario (4.98). This suggests that f_b is more critical in determining the overall compressive strength when full bedding is employed. There are two possible explanations for this observation. Firstly, full bedding distributes the load transfer path through both the mortar and the block interfaces. This distributed load path makes the overall compressive strength more reliant on the inherent strength of the masonry unit itself. Secondly, full bedding introduces more mortar joints, which can become weak points if the mortar has lower strength. This potential for weak mortar joints could make the overall strength less sensitive to variations in f_m compared to the masonry unit strength. Furthermore, the SHAP values for features such as prism geometry (L/t, H/t, and tm) were generally lower than those for f_b and f_m for full bedding. This could be attributed to the dominant influence of f_b in full bedding scenarios. When f_b plays a more significant role, the impact of these geometric and material properties might be overshadowed.

In contrast, feature importance in faceshell bedding exhibited a more balanced distribution. The SHAP values for f_b and f_m were closer (4.98 and 1.01, respectively) compared to full bedding, indicating that both the strength of the masonry unit and the mortar strength contribute more equally to the overall compressive strength. There are two possible explanations for this trend. Firstly, faceshell bedding concentrates the load transfer path on the mortar-block interfaces. This more defined load path could make the overall strength more sensitive to both the strength of the masonry unit (f_b) and the mortar (f_m). Secondly, the defined load transfer path in faceshell bedding might make the overall strength slightly less dependent on the prisms' specific geometric properties (L/t, H/t) compared to full bedding. The SHAP value for t_m was also lower in faceshell bedding (0.07) compared to full bedding (0.16). This aligns with the concept that faceshell bedding uses significantly less mortar overall.

4.5 Feature importance for the prediction

In optimising the compressive strength of hollow masonry prisms, feature importance analysis using XGB offers valuable insights. Once the XGBoost model is trained, the calculated feature importance scores are retrieved, as shown in Fig. 19. This analysis reveals a distinct trend: the fb emerges as the most dominant factor influencing the overall compressive strength of the prism (75.4% importance). This finding aligns with established principles, as stronger blocks naturally contribute to a more robust overall structure. The f_m (8.6% importance) also plays a role. As the binding agent, mortar strength influences how effectively forces are transferred between blocks. Following in importance was H/t ratio (5.3% importance). A higher H/t ratio can increase buckling under compression, reducing the prism's strength. This highlights the crucial role of maintaining a balanced geometry during the design process. The remaining features – t_m, L/t, α, and bedding type – accounted for a combined importance of 10.8%. This suggests that, within a reasonable range, these factors may not significantly affect the compressive strength as long as the primary factors are considered. These findings align with previous research, highlighting the importance of selecting high-fiber blocks and fine mortar for critical applications and maintaining a proper H/t ratio during the design phase.

Feature importance analysis examines the impact of removing individual input variables on the performance of a machine learning model predicting compressive strength. As XGB outperformed other models, the XGB model was considered for feature importance analysis. Figure 20; Table 5 demonstrate the predicted vs. actual compressive strength and performance indicators, respectively, for each case.

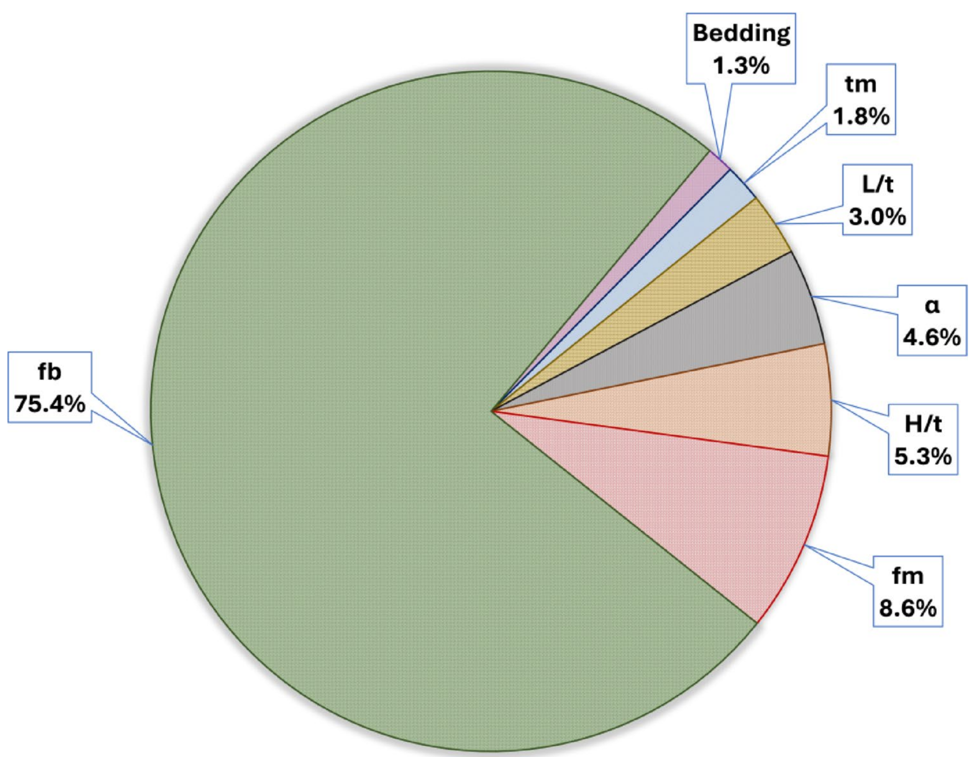

Fig. 19 Feature contribution for the prediction of compressive strength of hollow masonry prisms

Fig. 20 Predicted vs. actual compressive strength for model with one less parameter (**a**) none of the input removed, (**b**) f_b, (**c**) f_m, (**d**) t_m, (e) H/t, (**f**) L/t, (**g**) α, and (**h**) bedding type

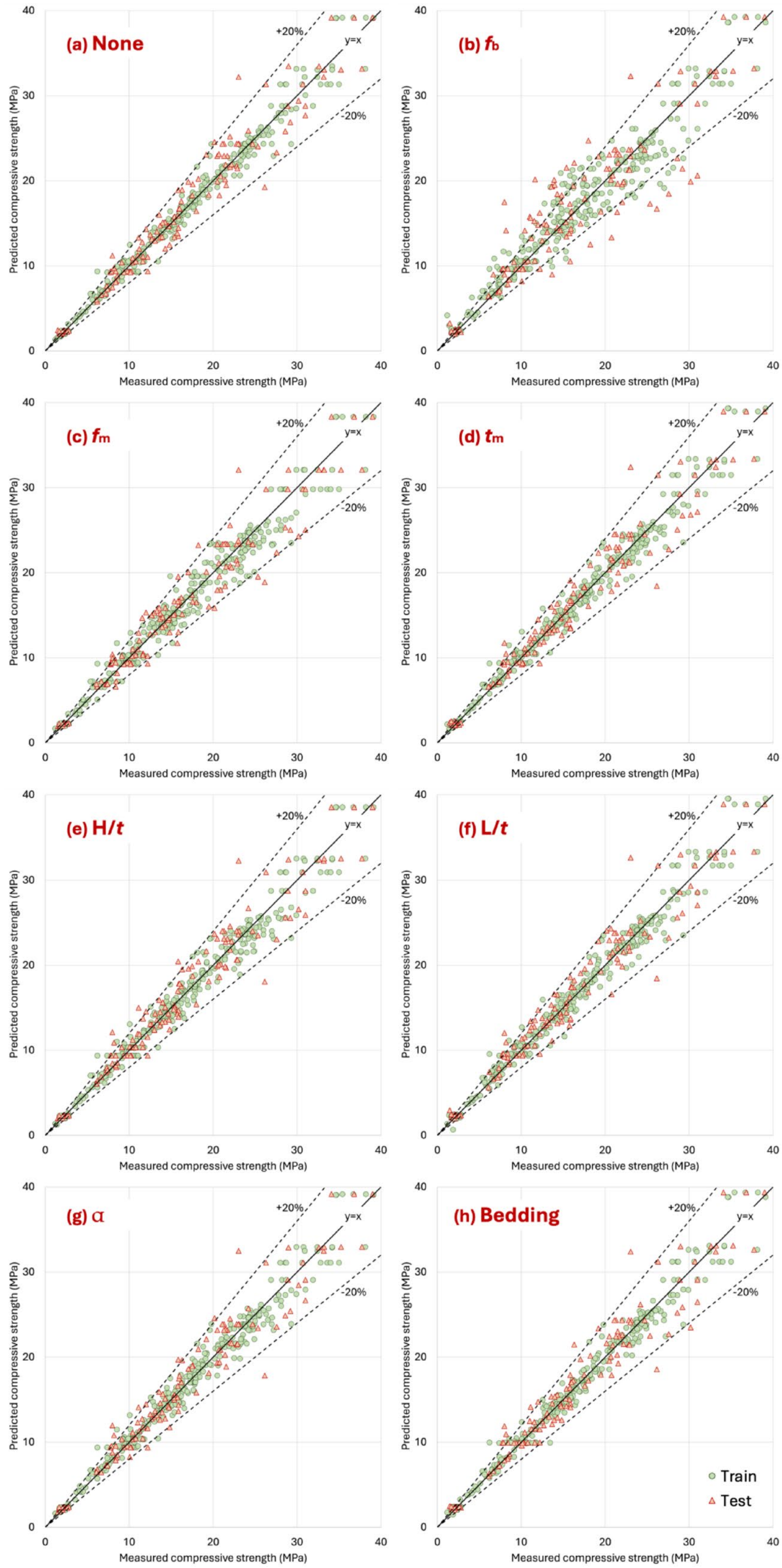

Table 5 Performance indicator for models with one less input variable

Removed parameter	Train					Test					Rank
	R^2	RMSE	MAE	SI	a20	R^2	RMSE	MAE	SI	a20	
None	0.98	1.17	0.72	0.07	0.97	0.95	2.06	1.44	0.12	0.92	
f_b	0.94	2.13	1.51	0.13	0.86	0.85	3.64	2.54	0.22	0.67	1
f_m	0.97	1.60	1.13	0.10	0.96	0.94	2.36	1.68	0.14	0.88	2
t_m	0.98	1.29	0.86	0.08	0.96	0.95	2.11	1.47	0.13	0.89	6
H/t	0.98	1.42	0.95	0.09	0.97	0.95	2.21	1.56	0.13	0.91	3
L/t	0.98	1.29	0.86	0.08	0.96	0.95	2.15	1.51	0.13	0.88	5
α	0.98	1.33	0.91	0.08	0.97	0.95	2.16	1.48	0.13	0.87	4
Bedding	0.98	1.25	0.83	0.08	0.96	0.95	2.22	1.50	0.13	0.88	7

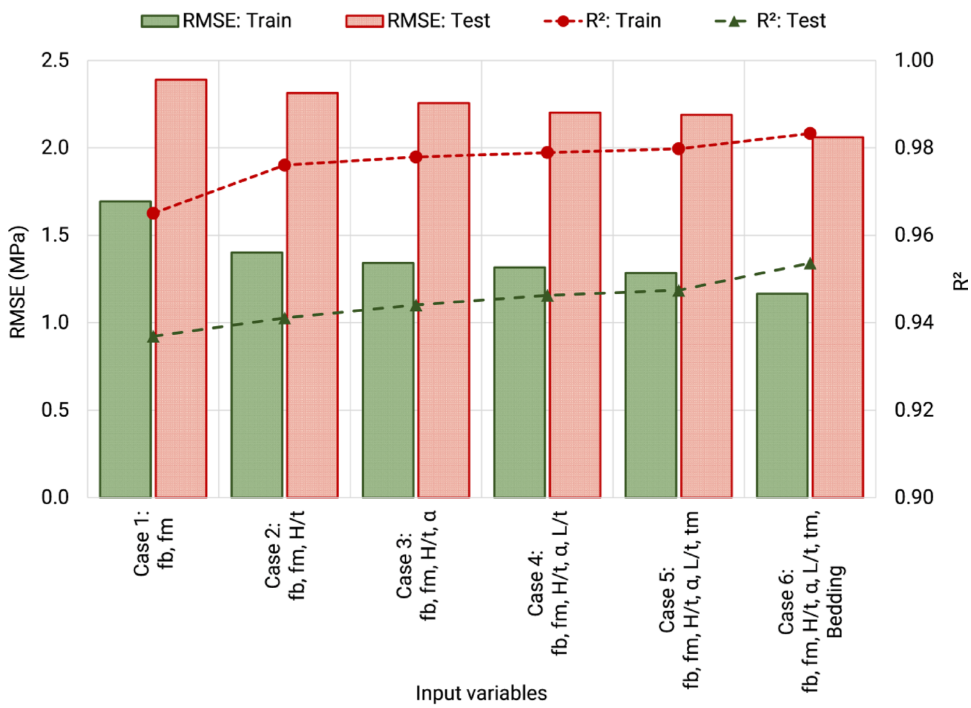

Fig. 21 Performance indicators variation for the various combinations of input variables

Removing f_b leads to the most significant increase in RMSE for training and testing data (almost double the error compared to the model, including all the input variables). Similarly, the fraction of data within the 20% error line decreases substantially (by around 30%) for both datasets. This suggests that f_b is the most influential variable for the model's prediction accuracy. Removing FM also results in a noticeable increase in RMSE (37% for the training dataset and 15% for the testing dataset, respectively) and a decrease in the fraction of data within the 20% error line (1% for the training dataset and 4% for the testing dataset, respectively) for both datasets. This indicates f_m plays a significant role in the model's performance.

Removing the bedding type shows a minor increase in RMSE (7% for the training dataset and 8% for the testing dataset, respectively) and a slight decrease in the fraction of data within the 20% error line for both datasets. This suggests Bedding has a minimal influence on the model's accuracy. Removing other variables (t_m, H/t, L/t, α) resulted in a minor increase in RMSE (round 10–14% for training and 3–7% for testing datasets, respectively) and a minor decrease in the fraction of data within the 20% error line (around 1–4% decrease) for both datasets. This suggests these variables have a less significant impact on the model's performance than f_b and f_m. Based on the analysis, the order of influence for the input variables on the compressive strength prediction model is likely: f_b (most influence), f_m, H/t, α, L/t, t_m, and bedding type (least influence).

The study further investigated the effectiveness of a simplified XGB model for predicting f_{mp} using only the most essential features identified through feature importance analysis. Real-world applications often face challenges acquiring all data points, making this approach highly relevant. Figure 21 illustrates the model's performance with various combinations of features.

The analysis began by identifying the most influential features. These features were then progressively incorporated into the model, starting with those deemed most

Table 6 This summarizes the machine learning models used to predict Hollow masonry compressive strength

Reference	Input variable	ML used	Number of datasets	Best ML model	Performance indicator - Training dataset	Performance indicator - Testing dataset	Feature importance
Ho and Tran [35]	f_b, f_m, H/t, f_m/f_b	GB	102	GB	$R^2=0.977$ RMSE = 0.803 MPa	$R^2=0.976$ RMSE = 0.906 MPa	$f_b > H/t > f_m > f_m/f_b$
Sharafati et al. [36]	f_b, f_m, H/t	BGR, DTR, SVR	90	BGR	$R^2=0.972$ RMSE = 0.670 MPa	$R^2=0.937$ RMSE = 1.229 MPa	-
Fakharian et al. [37]	f_b, f_m, H/t	ANN, GEP, GMDH	102	ANN	$R^2=0.903$ RMSE = 0.1.720 MPa	-	$f_b > f_m > H/t$
Present study	f_b, f_m, t_m, H/t, L/t, α, bedding	ANN, BT, KNN, RF, SVR, XGB	511	XGB	$R^2=0.98$ RMSE = 1.17 MPa	$R^2=0.95$ RMSE = 2.06 MPa	$f_b > f_m > H/t > L/t > \alpha > t_m$ >bedding

f_b: compressive strength of masonry unit, f_m: compressive strength of mortar, t_m: thickness of the mortar, t: width of the masonry prism, H: height of the masonry prism, L: width of the masonry prism, α: net-to-gross area ratio of hollow block

GB: Gradient boosting, BGR: Bagging Regression, DTR: Decision tree regression, GEP: Gene Expression Programming, GMDH: Group Data Handling

impactful by the feature importance analysis (f_b and f_m in Case 1). As expected, incorporating more features improved prediction accuracy, as evidenced by higher R^2 and lower RMSE. However, the benefit of adding additional features diminished after Case 2, which utilized the three features f_b, f_m, and H/t. This three-feature combination achieved an RMSE of approximately 1.40 MPa for the training dataset and 2.31 MPa for the testing dataset. Adding just one more feature (α) further improved performance to 1.34 MPa (training) and 2.26 MPa (testing), approaching the accuracy achieved by using all features. These results indicate that while using all available data improves model accuracy, a smaller set of key features, identified through feature importance analysis, retains substantial predictive power. This is advantageous when collecting all data points is impractical.

5 Comparison with published literature

In Table 6, different machine learning models were compared for predicting the compressive strength of hollow masonry. The models utilized various input variables, including the compressive strength of masonry units (f_b), mortar strength (f_m), mortar thickness (t_m), and other physical properties such as the height and width of masonry prisms (H/t, and L/t). Consequently, the predictions made by the models are sensitive to the chosen parameters, which is reflected in the performance metrics observed in the study. To better understand the influence of these initial assumptions, the performance of the models was compared with that of models developed by other researchers in the field. For example, Ho and Tran [35] employed Gradient Boosting (GB), achieving an R^2 of 0.977 for the training set and 0.976 for the test set. Their model focused on input variables such as the compressive strength of masonry units (f_b), mortar strength (f_m), and the height-to-thickness ratio (H/t). Similarly, Sharafati et al. [36] explored multiple machine learning techniques, including Bagging Regression (BGR), Decision Tree Regression (DTR), and Support Vector Regression (SVR), with BGR emerging as the best-performing model, yielding an R^2 of 0.972 on the training set and 0.937 on the test set. Fakharian et al. [37] utilized Artificial Neural Networks (ANN), Gene Expression Programming (GEP), and Group Method of Data Handling (GMDH), with ANN achieving the best results, yielding an R^2 of 0.903 on the training set.

In contrast, this study adopted a more comprehensive approach, utilizing a broader set of input variables and employing a range of machine learning techniques. Among these models, XGB performed the best, achieving an R^2 of 0.98 on the training set and 0.95 on the test set, with RMSE values of 1.17 MPa and 2.06 MPa, respectively. This performance comparison underscores the importance of selecting appropriate input variables and model techniques. Furthermore, the importance of each feature in the model was evaluated, revealing that the compressive strength of the masonry unit (f_b) had the most significant influence on predictions, followed by mortar strength (f_m), the height-to-thickness ratio (H/t), and other variables such as L/t and tm. These findings are consistent with those of Ho and Tran [35], who also identified f_b as the most significant feature in their model. The comparison with previous studies highlights the importance of model assumptions and initial parameters in determining predictive accuracy, demonstrating that even minor changes in input variables or assumptions can significantly impact model performance. This highlights the need for careful consideration of parameter choices when developing machine learning models, as they can substantially impact the outcomes of predictive tasks.

6 Limitation of the study and future research direction

While this study offers a significant advancement in predicting the compressive strength of hollow block masonry using machine learning, there are limitations for future research endeavours. The limitation of studies is:

- Data Source: The study emphasizes the importance of using a comprehensive dataset that includes all relevant factors. However, the research itself might be limited by the specific data source used. The generalizability of the findings could be enhanced by incorporating data from diverse sources and geographical locations, thereby accounting for potential variations in material properties and construction practices.
- Material Properties: While the study examines the impact of key material properties, such as block and mortar strength, it may not delve deeper into the specific material compositions or manufacturing processes. Including details like aggregate type, cement content, or curing conditions could provide even more nuanced insights.
- Model Explainability: Although the study employs feature importance analysis to identify influential factors, a deeper understanding of the model's internal workings could be valuable. Techniques like LIME (Local Interpretable Model-Agnostic Explanations could provide more granular explanations for specific predictions.
- Generalizability of Machine Learning Model: The high accuracy achieved by the XGB model might be specific to the dataset used for training and validation. Testing the model on entirely new datasets from different sources would be crucial to assess its generalizability in real-world scenarios.

Building upon the success of this study in utilizing machine learning for predicting compressive strength, several promising avenues for further research exist. The following are potential future directions that can expand upon the current knowledge base and enhance the practical applications of machine learning in hollow block masonry construction.

- Incorporate Additional Factors: Future research could investigate the impact of other factors that may affect compressive strength, such as the presence of voids or imperfections in the blocks, the type of bedding material used, or the curing conditions of the mortar.
- Multi-Scale Modeling: Investigating the relationship between the microstructure of materials (blocks and mortar) and their mechanical properties using techniques such as finite element analysis can provide a deeper understanding of the factors influencing strength at a more fundamental level.
- Hybrid Approaches: Combining machine learning models with physics-based models could leverage the strengths of both approaches. Machine learning can capture complex relationships from data, while physics-based models can provide insights into the underlying physical processes.
- Real-Time Monitoring: Integrating sensors into masonry structures can enable real-time monitoring of health and performance. This data could be used to update machine learning models and improve their predictive capabilities.
- Automation and Optimization: By integrating the XGB model into design software, engineers could optimize material selection, wall thickness, and other design parameters for specific projects, leading to more efficient and cost-effective construction practices.

By exploring these promising research directions, the prediction model will enhance the accuracy and generalizability of machine learning models, paving the way for the development of more efficient and sustainable construction practices.

7 Conclusion

This study explored the application of machine learning for predicting the compressive strength of hollow block masonry. By incorporating a comprehensive dataset that encompasses all relevant factors and comparing various machine learning models with existing prediction methods, the following results are obtained.

- When comparing building codes, Eurocode offered better strength estimations than AS3700. However, the equation by Sarhat and Sherwood provided the most accurate predictions by considering the height-to-thickness ratio, making it a more reliable tool for predicting the compressive strength of hollow block masonry.
- Machine learning models demonstrated promise in predicting compressive strength, particularly the XGB model, which accurately predicted compressive strength. This approach surpasses the limitations of traditional methods by achieving high accuracy ($R^2 > 0.92$) and low error (RMSE < 2.14 MPa). While all models showed a slight drop in performance on unseen data compared to training data, XGB's overall accuracy and ability to capture complex relationships make it a valuable tool for compressive strength prediction.

- SHAP analysis revealed that block strength is the most influential factor, followed by mortar strength. Slender prisms (high H/*t* or L/*t*) and lower solid area ratio (α) in blocks tend to have lower strength. The impact of mortar thickness is complex; a moderate thickness can be beneficial, but excessive thickness can be detrimental. Understanding these factors is crucial for optimizing the design of hollow block masonry.
- Feature analysis using XGB revealed block strength as the most crucial factor for predicting compressive strength, followed by mortar strength and slenderness (H/t ratio). Other factors, such as mortar thickness and block solidity (α), had a lesser impact. Focusing on these key features during design and using a simplified model can still achieve good prediction accuracy, making the process more efficient.

Applying machine learning to predict compressive strength in hollow block masonry offers several advantages. It eliminates the need for destructive testing, saving time and resources. Additionally, engineers can optimize material selection, wall design, and construction practices by focusing on the key factors identified through feature importance analysis. This leads to improved structural performance, increased cost-effectiveness, and safer and more sustainable construction practices using hollow block masonry.

Authors' contributions Study conception and design: N.S and P.J; Data acquisition: N.S; analysis and interpretation of results: P.J; draft manuscript preparation: N.S and P.J; manuscript review & editing: N.S.

Funding Not applicable.

Data availability Data can be made available at the request of interested parties.

Code availability Not applicable.

Declarations

Conflicts of interest The authors declare that they have no conflict of interest.

Ethics approval Not applicable.

Consent to participate This article contains no studies with human participants or animals performed by any authors.

Consent for publication Not applicable.

References

1. Nilimaa J (2023) Smart materials and technologies for sustainable concrete construction. Developments Built Environ 15:100177. https://doi.org/10.1016/j.dibe.2023.100177
2. Sathiparan N, Anburuvel A, Muralitharan M, Kothalawala DAI (2022) Sustainable use of Coco pith in cement-sand mortar for masonry block production: mechanical characteristics, durability and environmental benefit. J Clean Prod 360:132243. https://doi.org/10.1016/j.jclepro.2022.132243
3. JJ del Coz Díaz, García Nieto PJ, Álvarez Rabanal FP (2011) A Lozano Martínez-Luengas, design and shape optimization of a new type of Hollow concrete masonry block using the finite element method. Eng Struct 33(1):1–9. https://doi.org/10.1016/j.engstruct.2010.09.012
4. Sathiparan N (2023) Performance of sustainable cement mortar containing different types of masonry construction and demolition wastes. Clean Technol Environ Policy. https://doi.org/10.1007/s10098-023-02681-2
5. Sathiparan N, Jeyananthan P (2023) Prediction of masonry Prism strength using machine learning technique: effect of dimension and strength parameters. Mater Today Commun 35:106282. https://doi.org/10.1016/j.mtcomm.2023.106282
6. Nasrollahzadeh K, Zare M (2020) Experimental investigation on axially loaded Adobe masonry columns confined by polymeric straps. Constr Build Mater 262:119895. https://doi.org/10.1016/j.conbuildmat.2020.119895
7. Thaickavil NN, Thomas J (2018) Behaviour and strength assessment of masonry prisms. Case Stud Constr Mater 8:23–38. https://doi.org/10.1016/j.cscm.2017.12.007
8. Sarhat SR, Sherwood EG (2014) The prediction of compressive strength of ungrouted hollow concrete block masonry. Constr Build Mater 58:111–121. https://doi.org/10.1016/j.conbuildmat.2014.01.025
9. Dymiotis C, Gutlederer BM (2002) Allowing for uncertainties in the modelling of masonry compressive strength. Constr Build Mater 16(8):443–452. https://doi.org/10.1016/S0950-0618(02)00108-3
10. Gumaste KS, Nanjunda Rao KS, Venkatarama Reddy BV, Jagadish KS (2007) Strength and elasticity of brick masonry prisms and wallettes under compression. Mater Struct 40(2):241–253. https://doi.org/10.1617/s11527-006-9141-9
11. Kaushik Hemant B, Rai Durgesh C, Sudhir KJ (2007) Stress-Strain Characteristics of Clay Brick Masonry under Uniaxial Compression, Journal of Materials in Civil Engineering 19(9) 728–739. https://doi.org/10.1061/(ASCE)0899-1561(2007)19:9(728)
12. Christy F, Shanthi M (2013) Experimental study on axial compressive strength and elastic modulus of the clay and fly ash brick masonry
13. Lumantarna R, Biggs David T, Ingham Jason M (2014) Uniaxial compressive strength and stiffness of field-extracted and laboratory-constructed masonry prisms. J Mater Civ Eng 26(4):567–575. https://doi.org/10.1061/(ASCE)MT.1943-5533.0000731
14. Costigan A, Pavía S, Kinnane O (2015) An experimental evaluation of prediction models for the mechanical behavior of unreinforced, lime-mortar masonry under compression. J Build Eng 4:283–294. https://doi.org/10.1016/j.jobe.2015.10.001

15. Kumavat HR (2016) An experimental investigation of mechanical properties in clay brick masonry by partial replacement of fine aggregate with clay brick waste. J Institution Eng (India): Ser A 97(3):199–204. https://doi.org/10.1007/s40030-016-0178-7
16. Sajanthan K, Balagasan B, Sathiparan N (2019) Prediction of compressive strength of stabilized Earth block masonry, advances in civil engineering 2019. 2072430. https://doi.org/10.1155/2019/2072430
17. Köksal HO, Karakoç C, Yildirim H (2005) Compression behavior and failure mechanisms of concrete masonry prisms. J Mater Civ Eng 17(1):107–115. https://doi.org/10.1061/(ASCE)0899-1561(2005)17:1(107)
18. Priestley MJN (1986) Seismic design of concrete masonry shear-walls. J Am Concrete Inst 83(1):58–68
19. Khalaf FM, Hendry AW, Fairbairn DR (1994) Study of the compressive strength of blockwork masonry. ACI Struct J 91(4):367–375
20. Martins ROG, Nalon GH, Alvarenga RCSSA, Pedroti LG, Ribeiro JCL (2018) Influence of blocks and grout on compressive strength and stiffness of concrete masonry prisms. Constr Build Mater 182:233–241. https://doi.org/10.1016/j.conbuildmat.2018.06.091
21. Sarhat SR, Sherwood EG (2013) The prediction of compressive strength of grouted hollow concrete block masonry based on the contributions of its individual components, 12th Canadian Masonry Symposium, Vancouver, British Columbia
22. Ouyang J, Wu F, Lü W, Huang H, Zhou X (2019) Prediction of compressive stress-strain curves of grouted masonry. Constr Build Mater 229:116826. https://doi.org/10.1016/j.conbuildmat.2019.116826
23. Camps-Valls G, Gerhardus A, Ninad U, Varando G, Martius G, Balaguer-Ballester E, Vinuesa R, Diaz E, Zanna L, Runge J (2023) Discovering causal relations and equations from data. Phys Rep 1044:1–68. https://doi.org/10.1016/j.physrep.2023.10.005
24. Sathiparan N, Jeyananthan P Predicting compressive strength of quarry waste-based geopolymer mortar using machine learning algorithms incorporating mix design and ultrasonic pulse velocity. Nondestructive Test Evaluation 1–24. https://doi.org/10.1080/10589759.2024.2304257
25. Sathiparan N, Jeyananthan P Predicting compressive strength of cement-stabilized Earth blocks using machine learning models incorporating cement content, ultrasonic pulse velocity, and electrical resistivity. Nondestructive Test Evaluation 1–25. https://doi.org/10.1080/10589759.2023.2240940
26. Kiani H, Nasrollahzadeh K (2023) Fuzzy logic approach for seismic fragility analysis of RC frames with applications to earthquake-induced damage and construction quality. Structures 55:1122–1143. https://doi.org/10.1016/j.istruc.2023.06.047
27. Katsigiannis S, Seyedzadeh S, Agapiou A, Ramzan N (2023) Deep learning for crack detection on masonry façades using limited data and transfer learning. J Build Eng 76:107105. https://doi.org/10.1016/j.jobe.2023.107105
28. Ahamed AJN, Yamani SS, Dissanayaka LS, Sathiparan N (2025) Predicting the strength of alkali-activated masonry blocks using machine learning models: geopolymer mortar with quarry waste, rice husk ash, and eggshell ash. J Build Pathol Rehabil 10(1):60. https://doi.org/10.1007/s41024-025-00573-0
29. Inqiad WB, Dumitrascu EV, Dobre RA, Khan NM, Hammood AH, Henedy SN, Khan RMA (2024) Predicting compressive strength of Hollow concrete prisms using machine learning techniques and explainable artificial intelligence (XAI). Heliyon 10(17). https://doi.org/10.1016/j.heliyon.2024.e36841
30. Nassar S, Baudrit C, Saliba J, Saiyouri N (2024) Predicting compressed Earth blocks compressive strength by means of machine learning models. Constr Build Mater 447:138135. https://doi.org/10.1016/j.conbuildmat.2024.138135
31. Alacali S, Karslioglu M, Aslan ZU, Doran B (2025) Comparative analysis of machine learning algorithms for predicting shear strength of URM walls. Mater Today Commun 47:113257. https://doi.org/10.1016/j.mtcomm.2025.113257
32. Haq MZU, Singh S, Vora T, Dasarathy AK, Bharti K, Das VSP, Ricciotti L (2025) Performance evaluation of geopolymer masonry units: a hybrid approach combining laboratory testing and AI modeling. Case Stud Constr Mater 23:e04961. https://doi.org/10.1016/j.cscm.2025.e04961
33. Asteris PG, Lourenço PB, Hajihassani M, Adami C-EN, Lemonis ME, Skentou AD, Marques R, Nguyen H, Rodrigues H, Varum H (2021) Soft computing-based models for the prediction of masonry compressive strength. Eng Struct 248:113276. https://doi.org/10.1016/j.engstruct.2021.113276
34. Sathiparan N (2024) Predicting compressive strength of grouted masonry using machine learning models with feature importance analysis. Mater Today Commun 41:110487. https://doi.org/10.1016/j.mtcomm.2024.110487
35. Ho LS, Tran VQ (2024) Evaluation and estimation of compressive strength of concrete masonry prism using gradient boosting algorithm. PLoS One 19(3):e0297364. https://doi.org/10.1371/journal.pone.0297364
36. Sharafati A, Haji Seyed Asadollah SB, Al-Ansari N (2021) Application of bagging ensemble model for predicting compressive strength of hollow concrete masonry prism. Ain Shams Eng J 12(4):3521–3530. https://doi.org/10.1016/j.asej.2021.03.028
37. Fakharian P, Rezazadeh Eidgahee D, Akbari M, Jahangir H, Taeb AA (2023) Compressive strength prediction of hollow concrete masonry blocks using artificial intelligence algorithms. Structures 47:1790–1802. https://doi.org/10.1016/j.istruc.2022.12.007
38. BS-EN-1996 (2005) -1-1, eurocode 6: design of masonry structures - Part 1–1: general rules for reinforced and unreinforced masonry structures. European Committee for Standardization, Brussels, Belgium
39. Casali MJC, Oliveira LA, Sakamoto C, Schankoski RA, Roberto L (2012) The effect of mortar bedding type and hollow concrete block geometry on the mechanical behavior of high-strength structural masonry, 15th International Brick and Block Masonry Conference, Florianópolis – Brazil
40. Sathiparan N, Anusari MKN, Samindika NN (2014) Effect of void area on hollow cement masonry mechanical performance. Arab J Sci Eng 39(11):7569–7576. https://doi.org/10.1007/s13369-014-1325-y
41. Al-Amoudi MAA, Alwathaf AH (2014) The behavior of hollow concrete block masonry under axial compression. J Eng Sci 3(2):32–53
42. Zhou Q, Wang F, Zhu F (2016) Estimation of compressive strength of hollow concrete masonry prisms using artificial neural networks and adaptive neuro-fuzzy inference systems. Constr Build Mater 125:417–426. https://doi.org/10.1016/j.conbuildmat.2016.08.064
43. Valdameri CZ, Coelho LF, Junior KM, Utzig M, Roman HR (2016) In: Modena C, Proto F, Valluzzi MR (eds) Compression behaviour of structural clay block prisms with different shell and web thickness. Brick and Block Masonry, CRC
44. Zavalis R, Jonaitis B, Lourenço PB (2018) Experimental investigation of the bed joint influence on mechanical properties of hollow calcium silicate block masonry. Mater Struct 51(4):85. https://doi.org/10.1617/s11527-018-1215-y
45. Fonseca FS, Fortes ES, Parsekian GA, Camacho JS (2019) Compressive strength of high-strength concrete masonry grouted prisms. Constr Build Mater 202:861–876. https://doi.org/10.1016/j.conbuildmat.2019.01.037

46. Liu C, Zhu C, Bai G, Quan Z, Wu J (2019) Experimental Investigation on Compressive Properties and Carbon Emission Assessment of Concrete Hollow Block Masonry Incorporating Recycled Concrete Aggregates, Applied Sciences
47. Caldeira FE, Nalon GH, Oliveira DS, Pedroti LG, Ribeiro JCL, Ferreira FA, Carvalho JMF (2020) Influence of joint thickness and strength of mortars on the compressive behavior of prisms made of normal and high-strength concrete blocks. Constr Build Mater 234:117419. https://doi.org/10.1016/j.conbuildmat.2019.117419
48. AbdelRahman B, Galal K (2020) Influence of pre-wetting, non-shrink grout, and scaling on the compressive strength of grouted concrete masonry prisms. Constr Build Mater 241:117985. https://doi.org/10.1016/j.conbuildmat.2019.117985
49. Li J, Zhou H, Chen W, Chen Z (2021) Mechanical properties of a new type. Recycled Aggregate Concrete Interlocking Hollow Block Masonry, Sustainability
50. Zahra T, Thamboo J, Asad M (2021) Compressive strength and deformation characteristics of concrete block masonry made with different mortars, blocks and mortar beddings types. J Build Eng 38:102213. https://doi.org/10.1016/j.jobe.2021.102213
51. Syiemiong H, Marthong C (2021) Compressive strength behaviour of low-strength hollow concrete block masonry prisms. Struct Eng Mech 80(6):689–699. https://doi.org/10.12989/sem.2021.80.6.689
52. JH, Chávez-Gómez J, Álvarez-Pérez M, Mesa-Lavista R, García-Cedeño FA, Carpio-Santamaría G, Fajardo-San-Miguel (2024) FD Yépez-Rincón, experimental dataset of masonry prisms with Hollow concrete blocks. Data Brief 53:110207. https://doi.org/10.1016/j.dib.2024.110207
53. Elmeligy O, AbdelRahman B, Galal K (2024) Experimental investigation of the compressive and shear behaviours of grouted and hollow masonry constructed with PVA fibre-reinforced mortar and grout. Constr Build Mater 415:134954. https://doi.org/10.1016/j.conbuildmat.2024.134954
54. Ghaderi A, Ginn HL, Mohammadpour HA (2017) High impedance fault detection: a review. Electr Power Syst Res 143:376–388. https://doi.org/10.1016/j.epsr.2016.10.021
55. Montesinos López OA, Montesinos López A, Crossa J (2022) Fundamentals of artificial neural networks and deep learning. In: Montesinos OA, López A, Montesinos López J, Crossa (eds) Multivariate statistical machine learning methods for genomic prediction. Springer International Publishing, Cham, pp 379–425
56. Berikol GB, Berikol G Chap. 7 - Predictive models in precision medicine, in: D. Barh (Ed.), Artificial Intelligence in Precision Health, Academic Press2020, pp. 177–188
57. Gallego AJ, Rico-Juan JR, Valero-Mas JJ (2022) Efficient k-nearest neighbor search based on clustering and adaptive k values. Pattern Recogn 122:108356. https://doi.org/10.1016/j.patcog.2021.108356
58. Dutta P, Paul S, Kumar A (2021) 25 - Comparative analysis of various supervised machine learning techniques for diagnosis of COVID-19. In: Tripathi SL, Balas VE, Mohapatra SK, Prakash KB, Nayak J (eds) Electronic devices, circuits, and systems for biomedical applications. Academic, pp 521–540
59. Guillen MD, Aparicio J, Esteve M (2023) Gradient tree boosting and the estimation of production frontiers. Expert Syst Appl 214:119134. https://doi.org/10.1016/j.eswa.2022.119134
60. Awad M, Khanna R (2015) Support vector regression, in: M. Awad, R. Khanna (Eds.), Efficient Learning Machines: Theories, Concepts, and Applications for Engineers and System Designers, Apress, Berkeley, CA, pp. 67–80
61. Hsieh W, Lee Y, Huang C (2005) Epsilon-SSVR: a smooth support vector machine for epsilon-insensitive regression. IEEE Trans Knowl Data Eng 17(05):678–685. https://doi.org/10.1109/TKDE.2005.77
62. Rodríguez-Pérez R, Bajorath J (2022) Evolution of support vector machine and regression modeling in chemoinformatics and drug discovery. J Comput Aided Mol Des 36(5):355–362. https://doi.org/10.1007/s10822-022-00442-9
63. Mesut B, Başkor A, Aksu NB (2023) Chap. 3 - Role of artificial intelligence in quality profiling and optimization of drug products, in: A. Philip, A. Shahiwala, M. Rashid, M. Faiyazuddin (Eds.), A Handbook of Artificial Intelligence in Drug Delivery, Academic Press pp. 35–54
64. Sathiparan N, Jeyananthan P, Subramaniam DN (2024) Surface response regression and machine learning techniques to predict the characteristics of pervious concrete using non-destructive measurement: ultrasonic pulse velocity and electrical resistivity. Measurement 225:114006. https://doi.org/10.1016/j.measurement.2023.114006
65. 3700 A (2018) TMasonry Structures, Standards Australia, Sydney NSW
66. Koksal HO, Karakoç C, Yildirim H (2003) Compressive strength of concrete hollow-block prisms. Studi E Ricerche 24:189–205
67. Zahra T, Dhanasekar M (2016) Prediction of masonry compressive behaviour using a damage mechanics inspired modelling method. Constr Build Mater 109:128–138. https://doi.org/10.1016/j.conbuildmat.2016.01.048
68. Bui D-K, Nguyen T, Chou J-S, Nguyen-Xuan H, Ngo TD (2018) A modified firefly algorithm-artificial neural network expert system for predicting compressive and tensile strength of high-performance concrete. Constr Build Mater 180:320–333. https://doi.org/10.1016/j.conbuildmat.2018.05.201
69. Sathiparan N, Jeyananthan P, Subramaniam DN (2023) Prediction of compressive strength of fly ash blended pervious concrete: a machine learning approach. Int J Pavement Eng 24(2):2287146
70. Simão ML, Videiro PM, Silva PBA, de Freitas Assad LP, Sagrilo LVS (2020) Application of Taylor diagram in the evaluation of joint environmental distributions' performances. Mar Syst Ocean Technol 15(3):151–159. https://doi.org/10.1007/s40868-020-00081-5
71. Pantò B I Caliò, 3 - Numerical modeling for the seismic assessment of masonry structures, in: T. Ferreira, H. Rodrigues (Eds.), Seismic Vulnerability Assessment of Civil Engineering Structures At Multiple Scales, Woodhead Publishing2022, pp. 85–126
72. Cabané A, Pelà L, Roca P (2023) Effect of cross section aspect ratio and bearing surfaces treatment on the compressive strength of solid fired clay brick specimens. Constr Build Mater 383:131397. https://doi.org/10.1016/j.conbuildmat.2023.131397
73. Mohamad G, Lourenço PB, Roman HR (2007) Mechanics of hollow concrete block masonry prisms under compression: review and prospects. Cem Concr Compos 29(3):181–192. https://doi.org/10.1016/j.cemconcomp.2006.11.003
74. Yadav A, Pal S (2023) The impact of mortar thickness and strength on the brick masonry prism: an investigation. Mater Today Proc 93:552–559. https://doi.org/10.1016/j.matpr.2023.10.035